

TOPICAL REVIEW • OPEN ACCESS

Manufacturing strategies for highly sensitive and self-powered piezoelectric and triboelectric tactile sensors

To cite this article: Hyosik Park *et al* 2025 *Int. J. Extrem. Manuf.* **7** 012006

View the [article online](#) for updates and enhancements.

You may also like

- [A ferroelectric nanocomposite-film-based device for harvesting energy from water droplets using both piezoelectric and triboelectric effects](#)
Huidrom Hemojit Singh and Neeraj Khare
- [A critical review on polyvinylidene fluoride \(PVDF\)/zinc oxide \(ZnO\)-based piezoelectric and triboelectric nanogenerators](#)
Chirantan Shee, Swagata Banerjee, Satyaranjan Bairagi et al.
- [Ultrasound-driven triboelectric and piezoelectric nanogenerators in biomedical application](#)
Fu-Cheng Kao, Shih-Feng Hung, Chang-Chi Yang et al.

Topical Review

Manufacturing strategies for highly sensitive and self-powered piezoelectric and triboelectric tactile sensors

Hyosik Park^{1,6} , Gerald Selasie Gbadam^{1,6}, Simiao Niu², Hanjun Ryu^{3,4,*} and Ju-Hyuck Lee^{1,5,*} 

¹ Department of Energy Science and Engineering, Daegu Gyeongbuk Institute of Science and Technology (DGIST), Daegu 42988, Republic of Korea

² Department of Biomedical Engineering, Rutgers University, Piscataway, NJ 08854, United States of America

³ Department of Advanced Materials Engineering, Chung-Ang University, Anseong 17546, Republic of Korea

⁴ Department of Intelligence Energy and Industry, Chung-Ang University, Seoul 06974, Republic of Korea

⁵ Energy Science and Engineering Research Center, Daegu Gyeongbuk Institute of Science and Technology (DGIST), Daegu 42988, Republic of Korea

E-mail: hanjunryu@cau.ac.kr and jhlee85@dgist.ac.kr

Received 31 May 2024, revised 22 July 2024

Accepted for publication 18 October 2024

Published 11 November 2024



CrossMark

Abstract

Piezoelectric and triboelectric effects are of growing interest for facilitating high-sensitivity and self-powered tactile sensor applications. The working principles of piezoelectric and triboelectric nanogenerators provide strategies for enhancing output voltage signals to achieve high sensitivity. Increasing the piezoelectric constant and surface triboelectric charge density are key factors in this enhancement. Methods such as annealing processes, doping techniques, grain orientation controls, crystallinity controls, and composite structures can effectively enhance the piezoelectric constant. For increasing triboelectric output, surface plasma treatment, charge injection, microstructuring, control of dielectric constant, and structural modification are effective methods. The fabrication methods present significant opportunities in tactile sensor applications. This review article summarizes the overall piezoelectric and triboelectric fabrication processes from materials to device aspects. It highlights applications in pressure,

⁶ Contributed equally to this work.

* Authors to whom any correspondence should be addressed.



Original content from this work may be used under the terms of the [Creative Commons Attribution 4.0 licence](https://creativecommons.org/licenses/by/4.0/). Any further distribution of this work must maintain attribution to the author(s) and the title of the work, journal citation and DOI.

touch, bending, texture, distance, and material recognition sensors. The conclusion section addresses challenges and research opportunities, such as limited flexibility, stretchability, decoupling from multi-stimuli, multifunctional sensors, and data processing.

Keywords: triboelectric, piezoelectric, tactile sensor, manufacturing, composite

1. Introduction

Piezoelectric, triboelectric, piezoresistive effects, and capacitance change-based tactile sensors, which convert mechanical stimuli into electrical signals, are rapidly developing technologies for various applications such as soft robotics [1–6], human–machine interfaces [7–13], wearable electronics [14–18], and touch display [19–22]. Examples of tactile sensor applications include pressure [23–28], touch [29–35], texture [36–38], bending [39–43], distance [44–48], vibration [49–53], and material identification [54–58]. These applications extend industrial usage by incorporating artificial intelligence (AI) (figure 1). Interest in tactile sensors focuses on enhancing sensitivity, decoupling environmental noise, miniaturization, and simplification to facilitate precise control of machine interfaces such as prosthetic hands, diagnostic devices, and touch devices. Piezoresistive sensors, which detect electrical resistance changes due to mechanical deformation, are one of the promising types of tactile sensors and have demonstrated high sensitivity, linear response, fast response time, easy integration with electronic circuits, and miniaturization through micro-fabrication [59–63]. Structuring strategies, such as developing soft concave and convex structures, can increase sensitivity. However, piezoresistive sensors inherently suffer from baseline drift, hysteresis behavior, and power supply issues [63, 64]. Silicon, metals, and conductive polymers are widely used, but resistance changes are also affected by temperature variations, posing additional challenges for extreme environments [64]. Capacitive sensors, another type of tactile sensor, measure capacitance changes caused by the deformation of the dielectric layer between two electrodes [65–69]. Capacitive sensors offer very high sensitivity, can detect small displacements, and are less influenced by temperature variations. Dielectric materials and nanomaterial-composite materials are utilized in their construction. However, capacitive sensors require proper packaging to minimize the effects of humidity and a continuous power supply [70].

Piezoelectric and triboelectric effects are promising candidates due to several advantages, such as self-voltage signal generation, high impedance, and versatile form factors. The piezoelectric effect generates voltage through mechanical stress due to the displacement of ions within non-centrosymmetric crystal structures, resulting in changes in the electric dipole moment [71]. Ceramics and polymers such as quartz [72, 73], zinc oxide (ZnO) [41, 74, 75], lead zirconate titanate (PZT) [40, 50, 76], barium titanate (BTO) [77, 78], bone [79, 80], peptide [81, 82], cellulose [83, 84], and polyvinylidene fluoride (PVDF) [28, 35, 38, 85] have been extensively studied. The self-voltage generating properties are practically beneficial for wearable, implantable, and

small-scale devices [86–88]. With high sensitivity and fast response times, piezoelectric sensors can detect dynamic pressure changes. Enhancing crystallinity, phase control, material development, and composite structures can improve the piezoelectric constant and flexibility. One of the major challenges is replacing lead-based ceramics. The triboelectric effect generates voltage through contact and separation between two different materials. Electronegativity difference is one of the key factors determining surface triboelectric charge generation [89]. Contact electrification and electrostatic induction allow current flow between two electrodes. Metals [90–92], polyurethane (PU) [93, 94], poly(vinylidene fluoride-trifluoroethylene) (PVDF-TrFE) [95–97], polydimethylsiloxane (PDMS) [98], polyvinyl chloride [34, 99, 100], polytetrafluoroethylene (PTFE) [101–103], solid-state electrolytes [104–106], melanin [107, 108], and high dielectric ceramic (e.g. calcium copper titanate) composites structure [78, 109, 110] are utilized as triboelectric materials to maximize charge transfer efficiency. Triboelectric sensors offer higher output voltage than other types of tactile sensors and can operate at low frequency ranges. Additionally, it is easy to facilitate highly flexible/stretchable structures with environmentally friendly materials. However, overcoming environmental conditions such as humidity remains a challenge.

This review summarizes the manufacturing strategies for highly sensitive and self-powered piezoelectric and triboelectric sensors in all these contexts. The first sections provide the working mechanisms of piezoelectric and triboelectric effects. The following sections highlight material synthesis, composite structure manufacturing, thermal treatment, surface treatment, and other fabrication methods. The latest research in sensor applications is introduced, including sensor fabrications, pressure and bending structural designs, texture and location recognition, material selections, and AI-integrated systems. Structures, mechanical dimensions, sensitivity, and material information are included for each case. The conclusion presents the current state of the field and potential opportunities, such as consideration of multimodal sensing, decoupling from other stimuli, and AI-based accuracy enhancement.

2. Manufacturing approaches for enhancing piezoelectric and triboelectric properties

2.1. Piezoelectric mechanism

The piezoelectric effect is a material-based phenomenon that relates mechanical stress and charge displacement within a material [73]. It is a reversible process, hence divided into two groups known as direct and indirect effects; the direct effect converts mechanical to electrical energy, while the

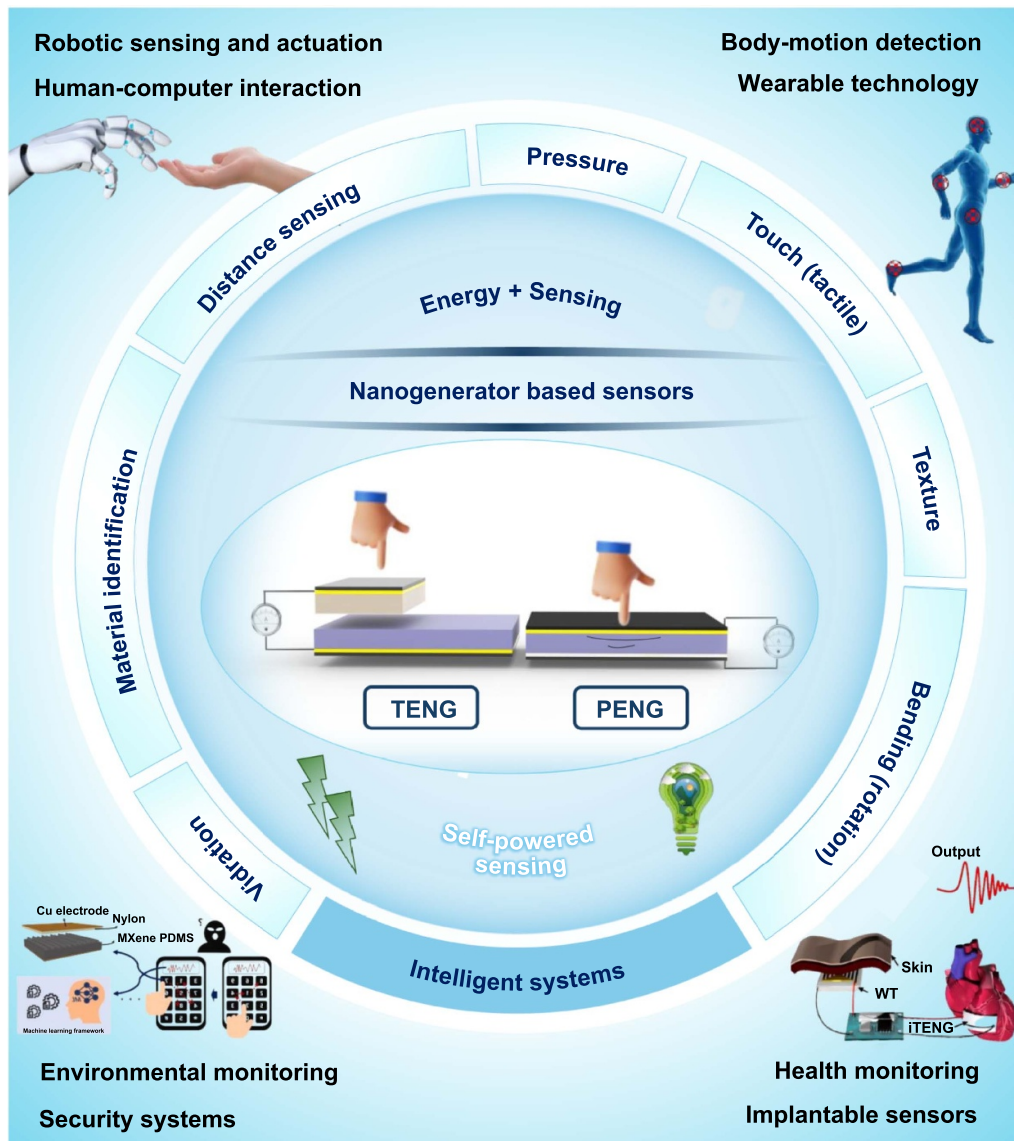


Figure 1. Schematic illustration of highly sensitive and self-powered sensing applications based on piezoelectric and triboelectric.

indirect effect (or inverse piezoelectric effect) converts electrical to mechanical energy. The direct effect is used for sensors and energy harvesting, while the indirect is used for actuation. Materials with non-centrosymmetric structures are at the forefront of this phenomenon; however, not all non-centrosymmetric materials exhibit the piezoelectric effect. Piezoceramics exhibit high electrochemical efficiency but are limited by their brittleness, which restricts their broad application. While piezopolymers address the challenge of flexibility, they result in less efficient energy conversion [111]. However, some organic materials can have piezoelectric properties and extended functionality to be biocompatible, making them suitable for *in-vivo* applications, although they have even lower piezoelectric coefficients [112]. Semiconductor-based piezoelectrics can generate direct current (DC) [113] and easily integrate into modern electronic circuits, but they also face the bottleneck of low piezoelectric coefficients, environmental

influences causing noise, and higher costs [114]. In all these types of piezoelectric materials, the basic principle of piezoelectricity remains converting mechanical energy by inducing dipoles in the materials to produce electricity and vice versa, each with their own benefits and drawbacks.

Without perturbation, the dipoles within piezoelectric materials are individually unidirectional, resulting in lower overall polarization, as shown in figure 2(a). Poling is used to align these dipoles in a favorable direction. This process involves applying a strong DC electric field slightly below the curie temperature, aligning the domains in piezoelectric materials. This alignment results in a net dipole moment and permanent remnant polarization, enhancing the piezoelectric properties. Figure 2(a) illustrates the stress application cycle for a typical piezoelectric material under a vertical compressive force. Without stress, there is no electrical output; thus, no electrical response is observed. However, when

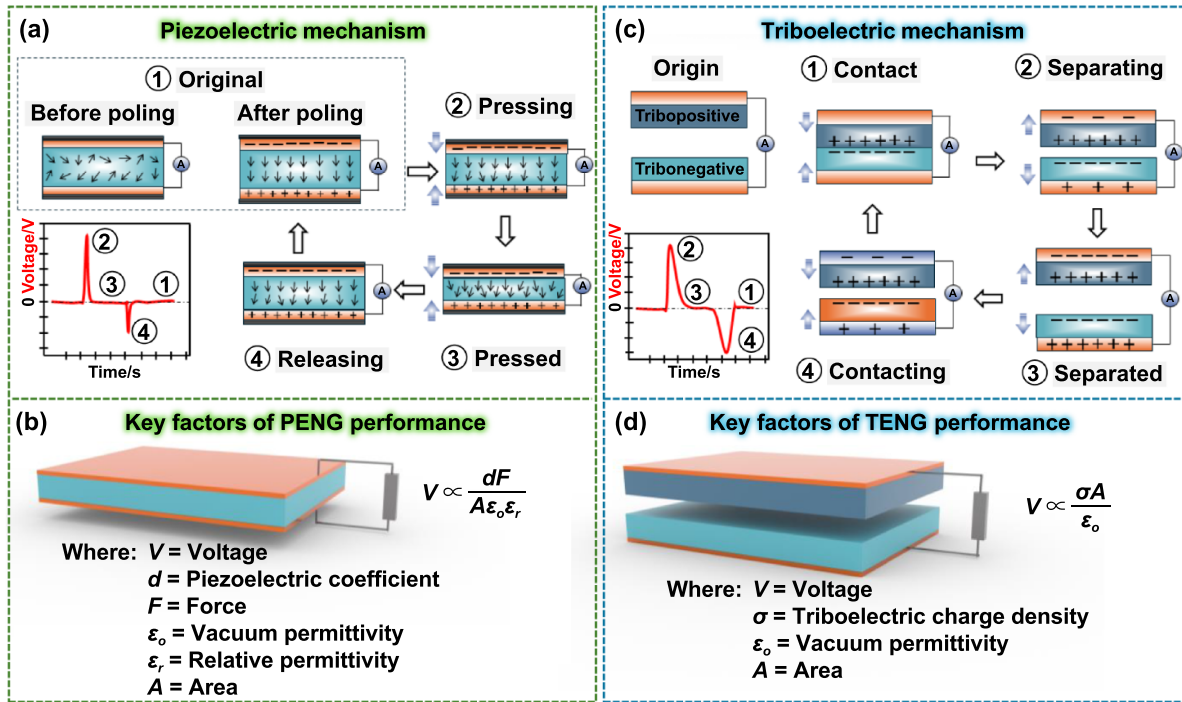


Figure 2. Mechanism of piezoelectric and triboelectric. (a) Working principle of piezoelectric nanogenerator (PENG). (b) Key factors of PENG output performance. (c) Working principle of triboelectric nanogenerator (TENG). (d) Key factors of TENG output performance.

stress is applied, the piezoelectric tensor is perturbed, generating an electric charge across the electrodes. Upon instantaneous removal of the stress, a rebound charge is produced in the opposite direction, restoring the initial charge equilibrium. This process results in an alternating current (AC) output.

There are four key factors affecting piezoelectric output performances (figure 2(b)). These factors are the piezoelectric coefficient, force, effective area, and permittivity of piezoelectric materials. The piezoelectric coefficient (d) is the amount of electrical charge generated per unit of mechanical stress applied or the mechanical strain produced per unit of electric field applied. It is expressed in units of coulombs per newton ($C \cdot N^{-1}$) or meters per volt ($m \cdot V^{-1}$). The piezoelectric coefficient can be enhanced by changing crystal structures, poling process, material composition, temperature, and mechanical stress [115]. The applied force (F) induces the deformation of crystal structures in the piezoelectric material. When this force is increased, it leads to a larger charge displacement within the material, thereby resulting in a stronger electric dipole. Consequently, this enhanced dipole strength leads to higher output performance from the piezoelectric material [116]. The effective area of a piezoelectric material is the portion involved in energy conversion under mechanical stress. When the pressure is the same, an increase in the effective area allows for more charge to accumulate during deformation, thereby facilitating greater charge displacement and enhancing output performance [117]. The permittivity (ϵ) quantifies the capacity of a material to store electric charge in response to an electric field, indicative of a piezoelectric material's ability to retain electric polarization. With increased permittivity, the

capacitance of the piezoelectric material is enhanced, enabling it to hold a greater charge at a constant voltage level, which in turn reduces the output voltage [118]. Among the four key factors enhancing piezoelectric nanogenerator (PENG) output, the studies are focused on developing materials that increase the piezoelectric coefficient. The piezoelectric coefficient is critical for assessing the performance of piezoelectric materials in applications such as sensors, actuators, and energy harvesting devices. Enhancements in the piezoelectric coefficient directly impact the efficiency and functionality of these technologies.

2.2. Manufacturing strategies for high piezoelectric constant materials

As previously mentioned, piezoelectric output voltage is proportional to its piezoelectric constant and strain. Thus, enhancing the piezoelectric constant is crucial for improving the sensitivity of tactile sensors. This section details manufacturing strategies developed for lead-based and lead-free piezoceramic, piezopolymer, and piezocomposite materials, all of which exhibit high piezoelectric constants.

Figure 3(a) shows PZT that is manufactured by aerosol deposition to efficiently create dense, nano-grained polycrystalline ceramic thick films at room temperature, effectively preventing the cracking common in high-temperature processes [119]. The average granule size, particle size, and thickness of PZT are $100 \mu m$, $1.5 \mu m$, and $7 \mu m$, respectively. The piezoelectric properties are enhanced up

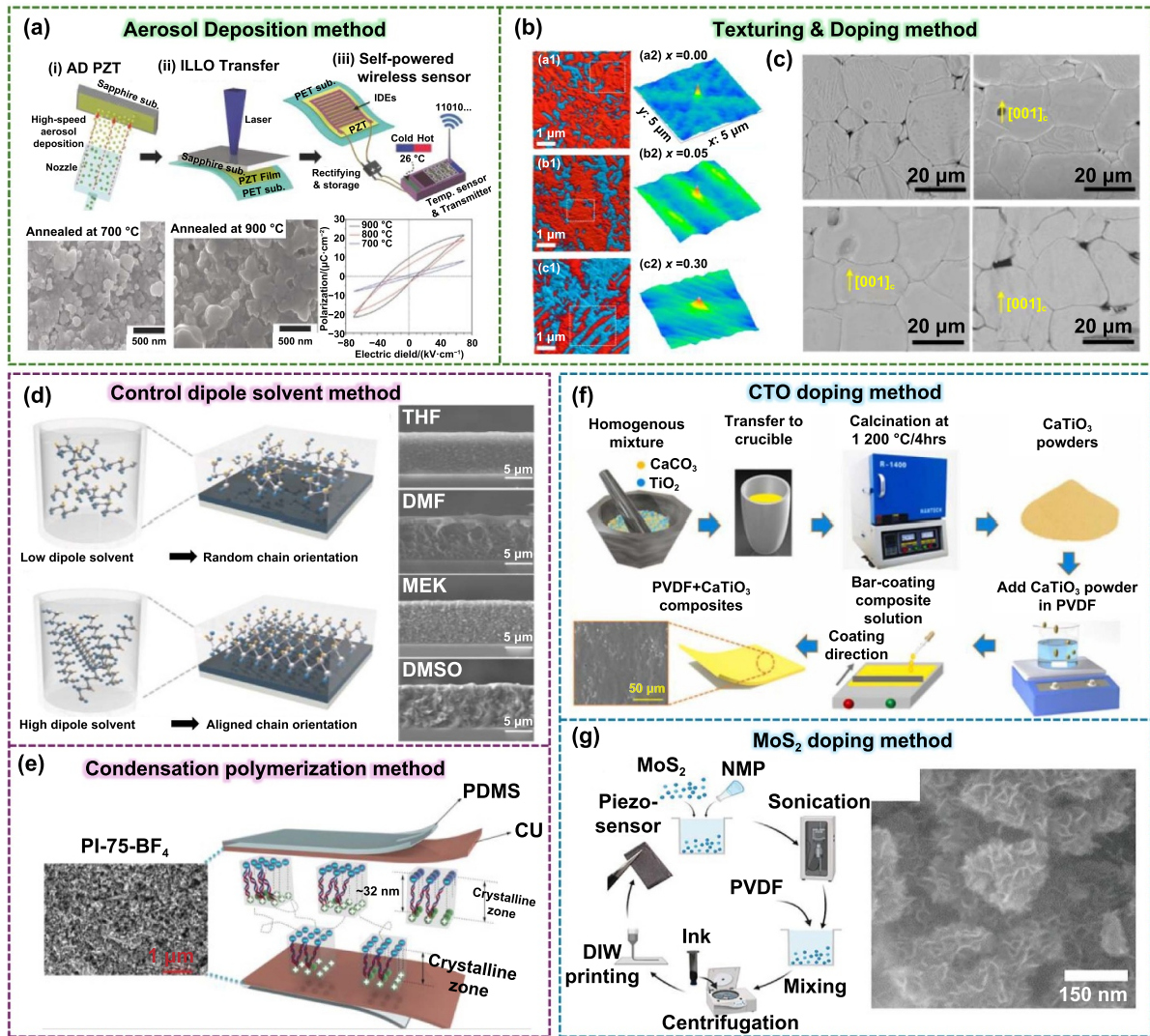


Figure 3. Manufacturing strategies for high piezoelectric constant materials. (a) Aerosol deposition manufacturing for nano-grained polycrystalline lead zirconate titanate (PZT). [119] John Wiley & Sons. © 2016 WILEY-VCH Verlag GmbH & Co. KGaA, Weinheim. (b) Texture engineering and Sm modification process for lead-free piezo-ceramics (Na, K)NbO₃-based doped Sm. Reprinted with permission from [120]. Copyright (2023) American Chemical Society. (c) Templated grain growth method for oriented grains of BaTiO₃-based doped LiCo₃. Reprinted with permission from [121]. Copyright (2023) American Chemical Society. (d) Solvent controlling method for higher crystallinity and dipole alignment P(VDF-TrFE). [95] John Wiley & Sons. © 2017 WILEY-VCH Verlag GmbH & Co. KGaA, Weinheim. (e) Condensation polymerization method for copolyimide doped ionic liquid [122]. Reprinted from [122], © 2019 Elsevier Ltd. All rights reserved. (f) Piezoceramic CaTiO₃ doping process for PVDF CTO piezoelectric composite film [123]. Reprinted from [123], © 2022 Elsevier Ltd. All rights reserved. (g) 3D printing process for PVDF-based doped MoS₂ piezoelectric composite ink. Reproduced with permission from [124]. © 2023 The Authors. Advanced Functional Materials published by Wiley-VCH GmbH. CC BY-NC-ND 4.0

to $d_{33} = 406 \text{ pC} \cdot \text{N}^{-1}$ by annealing the films at temperatures between 700 °C and 900 °C, optimizing crystallization and ferroelectric qualities while managing grain size to reduce interference between ferroelectric domains. Although PZT has a high piezoelectric constant, lead-free piezoceramics are required due to the toxicity of lead. Figure 3(b) details the creation of enhanced lead-free piezoceramics through texture engineering and samarium (Sm) modification, targeting improvements in (Na, K)NbO₃-based piezoceramics [120]. The ceramics are made by synthesizing NaNbO₃ templates through high-temperature stoichiometric reactions, followed by uniformly mixing raw powders of K₂CO₃ (99.5%), Na₂CO₃ (99.99%), Nb₂O₅ (99.9%), Sb₂O₃ (99.99%), Bi₂O₃

(99.9%), Sm₂O₃ (99.99%), and ZrO₂ (99.0%), including templates by 12 h ball milling after calcination at 850 °C. 0.5 wt% of Fe₂O₃ (99.0%) is introduced to enhance the sintering process. Tape casting at a rate of $1 \text{ mm} \cdot \text{s}^{-1}$ fabricate a thickness of 0.25 mm. After pressing to make a ceramic disk (diameter of 10 mm, thickness of 1 mm), heat treatment and sintering at 750 °C for 2 h and 1080 ~ 1100 °C for 10 h, respectively, eliminate binder and grow textured grains. Doping with Sm notably increases the piezoelectric constant by inducing local structural heterogeneity ($d_{33} = 710 \text{ pC} \cdot \text{N}^{-1}$). Barium titanate (BaTiO₃), which is another lead-free textured ceramic, is fabricated with a manufacturing method using (Ba_{0.95}Ca_{0.05})(Ti_{0.92}Zr_{0.06}Sn_{0.02})O₃ (BCTZS) templated grain

growth enhanced by Li_2CO_3 , which lowers texturing temperatures and improves grain orientation (figure 3(c)) [121]. The BaTiO_3 -based ceramic undergoes doping with Li_2CO_3 , promoting heteroepitaxial nucleation of oriented BCTZS. Templated grains replace highly [001]c-oriented grains during growth processes. The coexistence of multiple crystal phases enables enhanced piezoelectric properties through improved anisotropy exploitation and polarization dynamics ($d_{33} = 820 \text{ pC}\cdot\text{N}^{-1}$).

Due to their brittle nature, piezoelectric ceramics are often unsuitable for wearable applications. As a result, piezopolymers such as PVDF are preferred for their flexibility. Figure 3(d) illustrates the manufacturing process for enhancing the piezoelectric constant of P(VDF-TrFE), which involves using solvents like tetrahydrofuran, methyl ethyl ketone, dimethylformamide (DMF), and dimethyl sulfoxide (DMSO) to dissolve the polymer [95]. These solvents critically influence the polymer's crystallinity and dipole alignment, enhancing its piezoelectric response. P(VDF-TrFE) dissolved in DMSO, a high dipole moment solvent, exhibits an increased piezoelectric response ($d_{33} = 24.54 \text{ pm}\cdot\text{V}^{-1}$). Figure 3(e) details the synthesis of a piezoelectric bulk copolyimide (PI-75-BF4) using a condensation polymerization method that incorporates a novel, soluble, and meltable imidazole ionic liquid [122]. The primary materials used in this synthesis are pyromellitic dianhydride and p-phenylenediamine. Through molecular engineering with the imidazole ionic liquid, which imparts strong polarity and thermal stability up to $150 \text{ }^\circ\text{C}$, the piezoelectric constant is significantly enhanced, reaching approximately $d_{33} = 420 \text{ pC}\cdot\text{N}^{-1}$. The production process includes preparing a PI-75-BF4/DMAc solution, applying it to a substrate, and subsequently thermally treating it to achieve the desired piezoelectric properties.

To leverage the high piezoelectric constant of piezoceramics along with the flexibility of piezopolymers, researchers are exploring piezoelectric composite materials that incorporate ceramic particles into a polymer matrix. The production process of a CaTiO_3 (CTO)-PVDF composite is shown in figure 3(f) [123]. The process begins with the synthesis of CTO powder through a solid-state reaction that combines calcium carbonate and titanium oxide, followed by calcination at $1200 \text{ }^\circ\text{C}$ for 4 h. This powder is subsequently blended with PVDF in an n-methyl-2-pyrrolidone (NMP) solvent, and thin, flexible films are formed using a bar coater. After drying to remove the solvents, the films are enhanced with 8 wt% CTO to significantly improve the piezoelectric properties by increasing the beta phase of PVDF. The interaction between CTO particles and PVDF at the interfaces boosts up the β -phase of the PVDF-8 wt% CTO composite film. Figure 3(g) introduces a method for producing piezoelectric sensors by 3D printing PVDF mixed with MoS_2 nanofillers, significantly enhancing piezoelectric properties [124]. MoS_2 is synthesized using a solvothermal process and mixed with PVDF in NMP to create a homogeneously dispersed printable ink using a high-speed mixer. The presence of MoS_2 increases the β -phase of PVDF. The printing process aligns PVDF dipoles by applying shear stress through the nozzle, increasing the β -phase

content and eliminating the need for additional poling, reaching up $d_{33} = 48.4 \text{ pC}\cdot\text{N}^{-1}$.

2.3. Triboelectric mechanism

Contact electrification, or the triboelectric effect, is a ubiquitous phenomenon that scientists have observed for a long time. It was, and partially still is, regarded as a nuisance in the environment because it can lead to sparks and electric breakdown, among many other negative outcomes. Since then, many scientists have investigated the mechanisms by which this phenomenon occurs and how it can be controlled. The debate lies between electron transfer, ion transfer, and material transfer, and several studies have shown the prevalence of each mechanism. This debate became even more pronounced in 2012 when Prof. Zhong Lin Wang's group demonstrated the generation of electricity by the triboelectric phenomenon [89]. Named the triboelectric nanogenerator (TENG), it can be described as an energy-harvesting device that converts mechanical energy into electrical energy. It combines the triboelectric effect and electrostatic induction to produce electrical energy. Maxwell's displacement current forms the basis of the current generation, described as a time-varying charge density in electrodes caused by the movement of two dielectric plates. The triboelectric effect occurs between any two materials, opening up a broad range of materials from which the TENG device can be built. It is a materials-based technology that relies solely on the material's tendency to lose or gain electrons. Typically, materials are arranged according to their tendency on the triboelectric series. The TENG is attractive because its basic operation converts mechanical energy into electrical energy. Mechanical energy is readily available in many cases, such as friction, vibration, and body movement, and it is one of the few forms of energy that can easily be voluntarily initiated by humans or occur naturally without causing harm to the environment.

The working mechanism of the contact separation mode of TENGs is described in four stages. As described in figure 2(c), when we pair two materials with two electrodes across a load, contact electrification occurs at the contact stage, and the materials lose or gain electrons based on their tendency: electrons are transferred from electron-donating materials to electron-accepting materials, causing the electrode on the opposite side to become charged by the established electric field. Upon release, electrons flow through the load to neutralize the charge and establish electrostatic balance, forming an AC; this cycle continues. This forms the basics of the theory of TENGs. In ideal conditions, every material and every different pair of materials used as TENGs have a unique output peculiar by peak form and magnitude (figure 2(d)). The dielectric materials used in TENGs are characterized by their surface charge density, dielectric constant, and surface area, which are known to widely influence the number of charges that are generated and transferred, leading to increased electricity generation. Effective surface area also falls among the device operation variables, which can influence the TENG output, with other factors being frequency, force, load, and

humidity. Studying the dependence of these variables not only influences the generating capacity of TENGs but also enables the use of TENGs as sensors. In TENGs, the output shape, direction, and magnitude are determinants that are exclusively studied for many sensing applications, which will be discussed further. Hence, the power-generating ability combined with the sensing features makes TENGs a preferred basis for the fabrication of self-powered tactile sensors.

2.4. Manufacturing strategies for efficient triboelectric surface charge generation

As can be rightly inferred from the basic governing equations for triboelectric output, the overall output power will increase when the triboelectric surface charge increases. Surface area and dielectric constant are also important factors that can influence the resulting sensitivity in triboelectric sensors. In the following section, we discuss various manufacturing methods that have been shown to increase the triboelectric surface charge and overall performance as efficient power harvesters and sensors.

Direct charge injection onto the surface of triboelectric materials and fabricating microstructures on the surface are promising manufacturing methods to enhance triboelectric properties. Sun *et al* used a two-step Ar and O₂ reactive ion etching (RIE) plasma treatment to etch the surface of PI to enhance triboelectric properties (figure 4(a)) [125]. The treatment process increased the effective contact area by creating a granular nanostructure on the surface and induced favorable oxygen-containing functional groups by oxygen plasma irradiation with a radio frequency power of 25 W for 180 s. The modulation of triboelectric properties was shown to be effective by adjusting the irradiation time and power, and it showed good stability (5.5% decrease) over a week.

To offer an improvement in the surface charge density without the drawback of material surface wear or mechanical property damage, Li *et al* showed that low energy irradiation can be used to tune the chemical structures and functional groups of triboelectric polymers (figure 4(b)) [126]. Polyimide(PI), polyethylene terephthalate (PET), PTFE, and fluorinated ethylene propylene (FEP) were treated by irradiation with doses ranging from 1×10^{15} to 1×10^{17} ions per cm² using a 400 kV ion implanter at room temperature. Most experiments employed 50 keV He ions with a 50 kV potential. The irradiation was directed onto aluminum-backed films with a less than 600 nm range. The ion irradiation process can be more significant for some materials, as PI was widely improved, PET showed moderate changes, while PTFE and FEP remained largely unaffected. For irradiation of 1×10^{16} ions per cm², a surface charge density of up to $332 \mu\text{C}\cdot\text{m}^{-2}$ was achieved for PI. The enhancement observed in PI is proposed to stem from the emergence of a strong electron-donating group on its surface. These functional groups are believed to arise from the conjugation effect between the benzene ring and the irradiation-induced functional group of-NHCOR. The surface charge was higher than the previously mentioned ICP and RIE methods and could display stability for more than 60 d.

The simplest way to maximize charge transfer between any two triboelectric layers is to increase their effective contact area. Various micro/nano structuring strategies have been developed to create a variety of patterned surfaces to increase the output performance of TENGs. Figure 4(c) shows the fabrication of a morphology-controllable wrinkled micro/nano hierarchical structure (WHS), which involves several steps, including nano transfer, molding, and buckling techniques [127]. Various studies have shown that these different morphologies (micropatterns, nanopatterns, and wrinkles) can improve triboelectric properties; however, this study uniquely integrates all these morphologies onto a single surface to create a superhydrophobic surface. A photolithographically fabricated micro mold provides a micropatterned structure on silicon elastomer, and a biaxially pre-strain elastomer is immersed in water at 90 °C for 2 h to form wrinkles. The WHS was designed to have a contact angle of 152.5°, showing its excellent water-repellency and fast recovery even after water was sprayed.

Focusing on triboelectric materials, various methods have been adopted to make and tune materials to have better properties favorable for achieving high triboelectric surface charges. Various methods, including general material synthesis, poling, and doping, have been employed for this effort. Given that the dielectric properties of materials can be easily tuned by these methods, dielectric polarization has been widely studied as a key to improving triboelectric surface charges because the surface charge is proportional to the relative permittivity of the triboelectric material. In a study by Sun *et al* (figure 4(d)), a strategy of ionic polarization and interfacial polarization is adopted to improve the triboelectric performance of chitosan film by carefully engineering the molecular and ionic properties [128]. The blending method, which is the most commonly used method for doping, was used with additives such as polyvinyl alcohol (PVA), chloride salts, hydrochloric acid (HCl), and sodium hydroxide (NaOH) to obtain an optimized blend at chitosan, PVA at 5:1, pH 7, with 1 wt% NaCl. PVA changes the crystalline structure and increases the boundary between the crystal and amorphous regions. Due to large amino and hydroxyl groups, chitosan easily forms hydrogen bonds. Metal ions in chitosan form bonds with the hydroxyl group, breaking down hydrogen bonds. By adding HCl, the reorientation of the polarized group is regulated. Thus, interfacial and ionic polarization enhance the dielectric constant of the chitosan blend, enhancing its triboelectric properties.

Simple inference is that summing multiple TENG devices by stacking and using electrical connections is a strategy to improve output performance. Tang *et al* used a low-cost and simple fabrication method to produce and analyze a stacked TENG with alternating layers of counter-arch and arch-shaped devices (figure 4(e)) [129]. The PDMS films were fabricated using an inverted Si wafer micro-pyramid mold, photolithography, and KOH etching. The pyramid structure of PDMS facilitates mechanically stable properties. The 3-layer proposed stacked TENG was shown to significantly improve performance due to its ability to absorb more energy compared to the simple arch structure. Furthermore, their spring

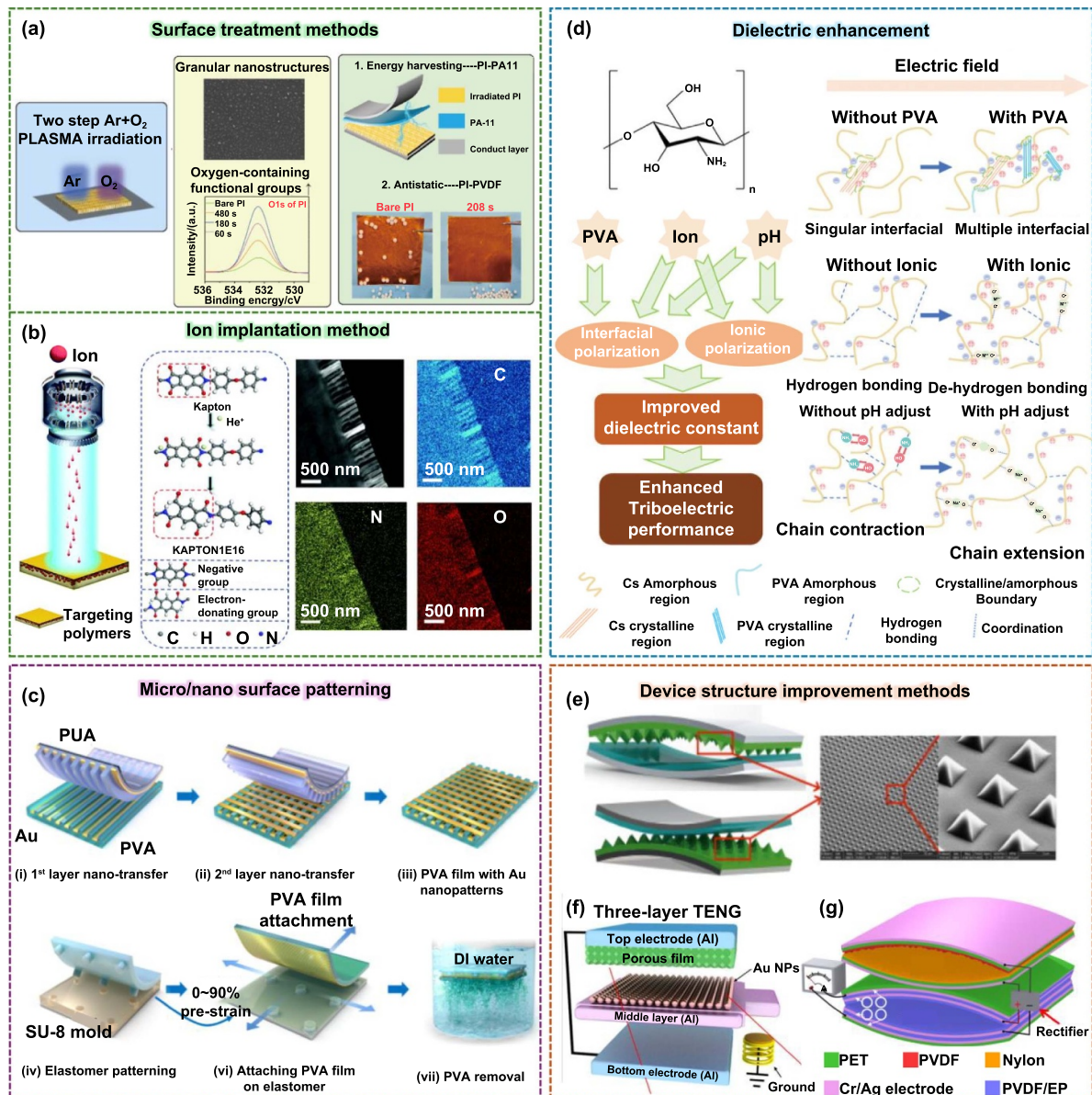


Figure 4. Manufacturing strategies for efficient triboelectric surface charge generation. (a) Plasma treatment to manufacture polyimide materials with enhanced triboelectric surface properties [125]. Reprinted from [125], © 2022 Elsevier Ltd. All rights reserved. (b) Low-energy helium ion irradiation process to fabricate polymers with enhanced charge density. Reproduced from [126] with permission from the Royal Society of Chemistry. (c) The fabrication process of wrinkled hierarchical structured film for a superhydrophobic TENG sensor [127]. Reprinted from [127], © 2021 Elsevier Ltd. All rights reserved. (d) Composite manufacturing to improve dielectric constant for a chitosan-based multi-modal sensing System. [128] John Wiley & Sons. © 2021 Wiley-VCH GmbH. (e) Fabrication of stacked arch-shaped TENGs with nanostructured surface to enhance output [129]. Reprinted from [129], Copyright © 2013 Elsevier Ltd. All rights reserved. (f) Manufacturing of three-layer structured TENG with a middle electric double layer to enhance output. Reproduced from [130]. CC BY 4.0. (g) Fabrication of PVDF and PA-6 based TENG with a multilayer self-improving structure to boost charge density and accumulation speed. Reproduced from [131]. CC BY 4.0.

structure further increases output signal duration, hence producing a continuous non-zero output during the oscillation process; this was studied in the range of 1 Hz–3 Hz.

Another layered TENG structure, shown in figure 4(f), presents an additional ground-connected structure between top and bottom electrodes for efficient charge separation [130]. The structure comprises Al and porous PDMS as tribo-friction layers, while an Au nanoparticle-deposited Al electrode serves as the middle layer connected to the ground. The output was

significantly enhanced up to 1.22 mA and 46.8 mW·cm⁻² by the middle layer, inducing an excess charge on the tribo surfaces based on volta's electrophorus.

Although the triboelectric charge is quantifiable, there lies more opportunity to increase energy harvesting efficiency through structural strategies, overcoming limitations such as air breakdown. Li Cheng *et al* reported a self-improving-TENG (SI-TENG) that could achieve a maximum effective charge density of 490 μC·m⁻², which is close to the highest

recorded charge density value in an air environment to the best of our knowledge (figure 4(g)) [131]. The SI-TENG with inner plane-parallel capacitor structure (PPCS) is made of parts I and II, fabricated using PET, Cr/Ag electrode PVDF, and PA-6 solutions with a simple spin-coating method. The improvement strategy involves a charge-filling technique by integrating and electrically connecting a rectifier bridge into the stacked TENG so that part I acts as a voltage source to fill the charge into the PPCS. The blocked charge within the rectifier is stored and released as an AC when the TENG is in operation. This study showed a good strategy for increasing charge density and charge accumulation speed in TENGs.

3. Manufacturing strategies for Piezoelectric-based intelligent sensor applications

Piezoelectric-based tactile sensors convert mechanical stimuli, such as pressure, bending, and roughness, into electrical signals. High sensitivity, decoupling from environmental noise signals, fast response times, and self-powered systems are essential for interactive interfaces, wearable electronics, and robotics. This section explores the materials, devices, and applications of tactile sensors that detect piezoelectric-based pressure, bending, and texture.

3.1. Piezoelectric-based pressure and bending sensors

Liu *et al* fabricated a flexible piezoelectric sensor based on an all-ceramic piezoelectric energy harvester using a sol-gel process, depositing PZT films on yttrium-stabilized zirconia (ZRC) substrates (figure 5(a)) [40]. This method enables high-temperature crystallization for forming PZT films while maintaining the flexibility required for dynamic applications like wearable sensors. The piezoelectric properties are optimized by enhancing the crystalline structure during film growth, particularly by developing a strong (001) texture on ZRC substrates that enhance domain switching behaviors, crucial for increasing the piezoelectric response. The sensor device is completed by depositing PZT films on ZRC, adding platinum/titanium interdigitated electrodes, and encapsulating the assembly in a protective polymer, making it durable and flexible for extensive mechanical deformation. As a sensor application, PZT film measures bending angles and muscle contraction. As a self-powered sensor, it responds linearly to strain (bending strain range 0.116%–0.214%) with a maximum open-circuit voltage of about 105 V and a short-circuit current of 0.58 μA , showcasing a significant potential for wearable technology and biomechanical energy harvesting.

Figure 5(b) discusses the development of piezoelectric sensors using $\alpha\text{-In}_2\text{Se}_3$ synthesized via chemical vapor deposition (CVD) [43]. Controlling the stacking configuration and polarization direction in 2D layers allows for high piezoelectric properties by preventing polarization cancellation between layers. The sensors are constructed by layering the synthesized material with integrated electrodes encapsulated in a protective polymer to ensure mechanical stability. These sensors

detect high sensitivity to mechanical strain changes (ranging from 0.21% to 0.62%), suitable for health monitoring applications like pulse and breath monitoring. Notably, the piezoelectric output and sensitivity increase with the number of layers, with a seven-layer sensor showing significantly greater responsivity (598.1 pA per 1% strain) than a monolayer, indicating robust performance suitable for real-time physiological monitoring.

Liu *et al* fabricated tactile sensors using a uniform-field electrospinning (UFES) process that fabricates nanofibrous strips (NFSs) on PU films (figure 5(c)) [132]. A uniform electric field is maintained between the aided metal plate and the collector, with the distance between the nozzle and collector set at 40 mm. This method controls fiber architecture, with the PVDF nanofiber thickness being 60 μm and a 1 mm distance between PVDF strips on the PU film (20 μm thick), crucial for consistent piezoelectric properties. The piezoelectric constant is enhanced by aligning fibers in a helical structure via UFES, improving stability (over 1000 cycles) and response under mechanical stress (generating 22.4 mV under 3 kPa pressure). The sensor device is constructed by layering NFSs in an orthogonal pattern, integrating electrodes, and mounting them on a PDMS substrate to form a 5×5 grid, encapsulated to maintain durability and flexibility. These sensors, sensitive to $7.1 \text{ mV}\cdot\text{kPa}^{-1}$, effectively detect and map pressure changes, making them ideal for wearable electronics and applications like electronic skins, showcasing their utility in interactive interfaces and real-time pressure tracking.

Figure 5(d) outlines the creation and performance of an environmentally friendly piezoelectric sensor made from bacterial cellulose (BC) hydrogel and imidazolium perchlorate (ImClO_4) [133]. BC hydrogel is synthesized using gluconacetobacter xylinus and purified with a sodium hydroxide solution, forming a highly crystalline, water-absorbent matrix. ImClO_4 is produced by combining imidazole with perchloric acid and allowing the mixture to evaporate, forming crystals with a high piezoelectric coefficient ($46 \text{ pC}\cdot\text{N}^{-1}$). The sensor is manufactured by embedding the BC hydrogel with ImClO_4 , which crystallizes within the hydrogel's network as the solvent evaporates. This hybrid material combines the flexibility and biodegradability of BC with the enhanced piezoelectric properties of ImClO_4 , resulting in a sensor that exhibits high sensitivity ($4.24 \text{ mV}\cdot\text{kPa}^{-1}$) across a broad operational range and superior mechanical durability. Additionally, the BC component is fully biodegradable, and ImClO_4 can be recycled, supporting the sensor's design focus on reducing environmental impact.

Figure 5(e) details the development of a muscle fiber-inspired piezoelectric textile, synthesizing BTO nanoparticles embedded within PVDF nanofibers via electrospinning, subsequently coated with PDA (3.02 wt% doping) [39]. This coating enhances mechanical strength and piezoelectric properties by improving the interfacial adhesion, which boosts piezoelectric performance by 47%. The fibers are fashioned into a non-woven textile with electrodes, forming a sensor that maintains its properties under extensive mechanical stress, suitable for wearable applications. The piezoelectric textile

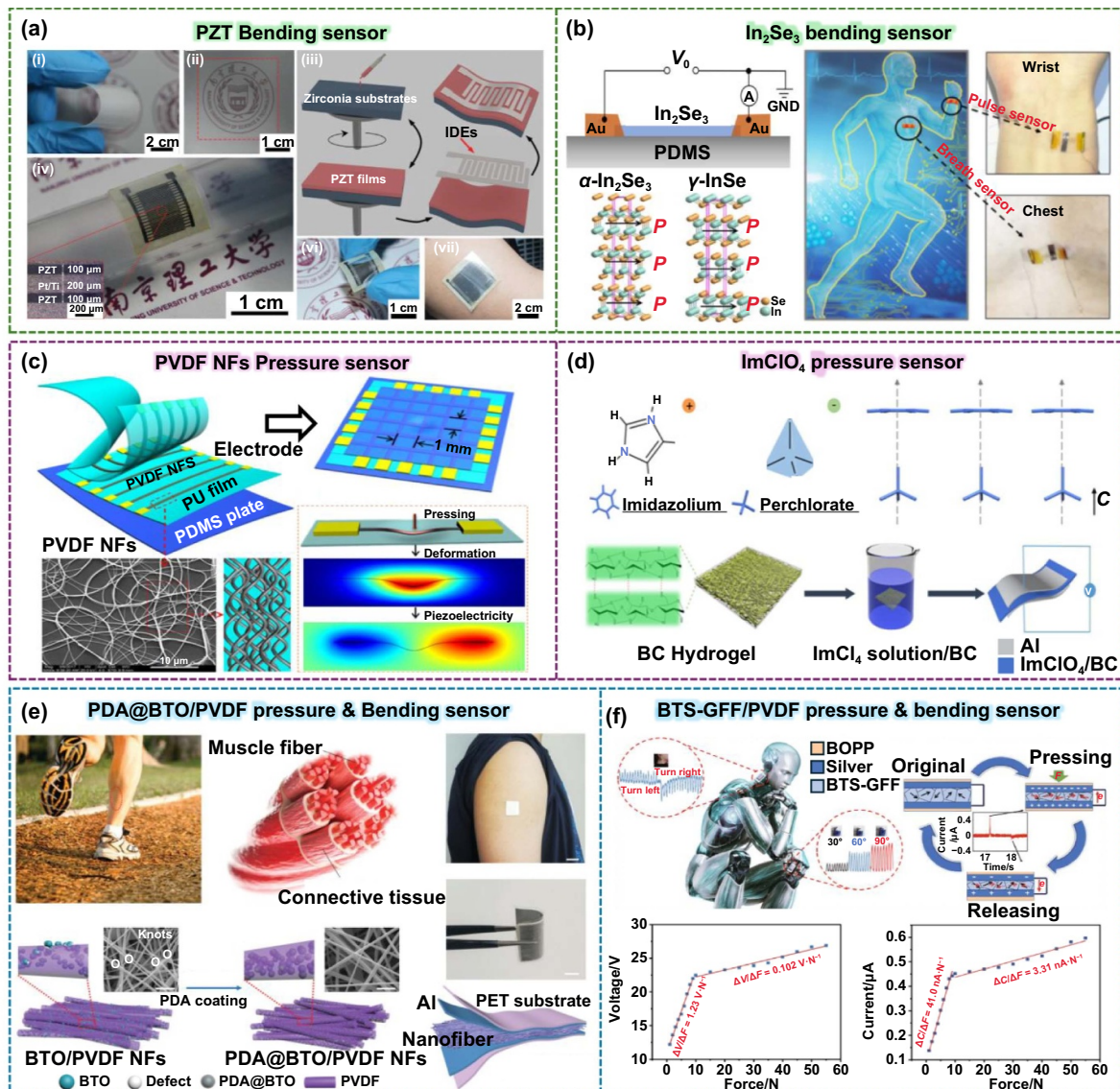


Figure 5. Manufacturing strategies of piezoelectric-based pressure and bending sensors. (a) Sol–gel process for a piezoelectric bending sensor based on PZT with zirconia substrate. [40] John Wiley & Sons. © 2022 Wiley-VCH GmbH. (b) CVD deposition method for a piezoelectric bending sensor based on In₂Se₃ 2D layer. Reprinted with permission from [43]. Copyright (2019) American Chemical Society. (c) Uniform-field electrospinning (UFES) process for a pressure sensor based on PVDF nanofiber. Reprinted with permission from [132]. Copyright (2021) American Chemical Society. (d) Embedding process for a pressure sensor based on bacterial cellulose (BC) with ImClO₄. Reprinted with permission from [133]. Copyright (2022) American Chemical Society. (e) Piezoelectric textile process with embedding for a pressure and bending sensor based on polydopamine@barium titanate/PVDF (PDA@BTO/PVDF). [39] John Wiley & Sons. © 2021 Wiley-VCH GmbH. (f) Sol–gel process for a pressure and bending sensor based on barium titanate stannate—glass fiber fabrics/PVDF (BTS-GFF/PVDF). Reproduced from [134]. CC BY 4.0.

exhibits significant sensitivity to pressure and bending, achieving a voltage sensitivity of 3.95 V·N⁻¹, which is ideal for dynamic physiological monitoring, including pulse and movement analysis. The sensor’s ability to endure repeated stress cycles without performance degradation (<3% degradation after 7400 cycles) and its heightened sensitivity make it highly effective for real-time physiological signal monitoring, such as human motion monitoring and active voice recognition, demonstrating potential for broad applications in health monitoring devices.

Figure 5(f) describes the development of barium titanate stannate-glass fiber fabrics/PVDF (BTS-GFF/PVDF) sensors, utilizing a sol–gel fabrication process and material properties to enhance piezoelectric performance [134]. BTS thin films are deposited onto glass fiber fabrics via a sol–gel method followed by spin coating, ensuring the formation of continuous, well-crystallized films on a flexible substrate. The optimization of the piezoelectric constant in these films is achieved by leveraging the low curie temperature of BTS, which enhances sensitivity to minute force changes, thereby enhancing the

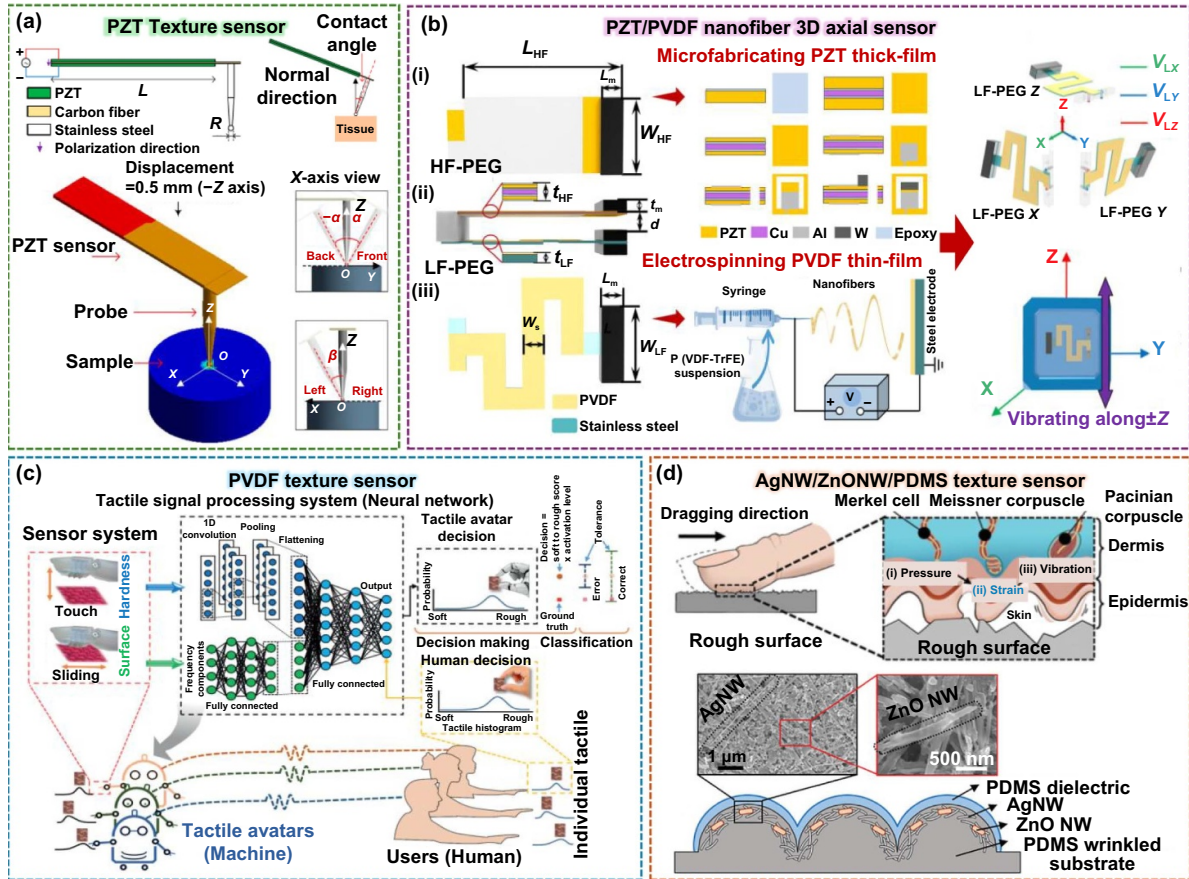


Figure 6. Piezoelectric-based texture and location sensors. (a) Bimorph structure for a texture sensor based on PZT. Reproduced from [76]. CC BY 4.0. (b) High and low frequency piezoelectric generator (HF-PEG, LF-PEG) for a 3D axial location sensor based on PZT/PVDF nanofiber. Reprinted with permission from [135]. Copyright (2023) American Chemical Society. (c) Mimicking human tactile cognition with deep learning for a texture sensor based on PVDF. Reproduced from [38]. CC BY 4.0. (d) Finger pad-inspired electronic skin for a texture sensor based on AgNW/ZnONW/PDMS. Reproduced from [37]. CC BY 4.0.

piezoelectric response under mechanical stress. To craft the sensors, a PVDF coating is applied to the BTS-GFF through spin coating, after which silver electrodes are incorporated via magnetron sputtering to create ultra-thin, flexible sensors. These sensors exhibit high voltage sensitivity ($1.23 \text{ V}\cdot\text{N}^{-1}$) and current sensitivity ($41.0 \text{ nA}\cdot\text{N}^{-1}$) at low force ranges (1–9 N), making them highly effective for detecting subtle movements such as falling water drops or joint movements. Their flexibility and thin profile make them ideal for wearable health monitoring devices, as they conform closely to human skin, enabling accurate monitoring of physiological movements.

3.2. Piezoelectric-based texture and location sensors

Zhang *et al* designed a piezoelectric tactile sensor for tissue stiffness detection with an arbitrary contact angle (figure 6(a)) [76]. The bimorph tactile sensor structure uses PZT, with a carbon fiber interlayer and a stainless-steel spherical probe tip, optimizing contact with tissue surfaces. The contact angle α refers to the angle between the sensor probe and the normal direction of the tissue surface. This configuration allows for dynamic responses to mechanical stresses, which are crucial for accurately sensing and differentiating textures.

As the probe moves across a surface, it measures changes in electrical impedance caused by variations in mechanical impedance, which directly affect the sensor's resonance frequency. These changes indicate different textures, allowing the sensor to recognize and classify them effectively. The sensor sensitivity, defined as the ratio between the resonant frequency shift and the change in stiffness of the material, is $134.11 \text{ Hz}\cdot\text{MPa}^{-1}$ in the range from 0.045 MPa to 0.649 MPa. Additionally, in a blind recognition test simulation, the recognition rate is 100% when the contact angle is randomly selected within 30° and 94.1% within 45° , which is 38.7% higher than the unoptimized sensor from a previous study. This capability to detect subtle differences in tissue stiffness at different angles enhances the sensor's utility in precise medical applications.

Huang *et al* suggested an intelligent cubic-designed piezoelectric AIoT node (iCUPE) that integrates energy harvesting and self-powered sensing modules (figure 6(b)) [135]. The cubic design allows orthogonal placement of three frequency up-conversion piezoelectric nanogenerators (FUC-PEGs), ensuring a response to vibrational energy sources from various directions. The iCUPE device consists of a micromachined PZT thick film-based high-frequency (HF) PEG and

a P(VDF-TrFE) nanofiber thin film-based low-frequency (LF) PEG. For the HF PEG fabrication, a layer of conductive epoxy was screen-printed onto the surface of a polished PZT ceramic chip. Two such PZT chips were then affixed to the upper and lower surfaces of a double-sided polished copper sheet. This assembly underwent heating to 150 °C and was bonded under a pressure of 0.1 MPa in a vacuum chamber for 5 h. The bonded bimorph PZT chip was then ground and polished to a thickness of 70–100 μm on each side. Electrodes were created by sputtering 50 nm of chromium and 950 nm of aluminum onto the top and bottom surfaces using a magnetron sputter machine. The cantilever shape was then formed by laser cutting, and a tungsten proof mass was attached to the end of the cantilever. For the LF PEG fabrication, a stainless steel sheet shaped in a meandering pattern was utilized as both the substrate and bottom electrode. The P(VDF-TrFE)/DMF/acetone mixture was electrospun directly onto this substrate to create a thin film of P(VDF-TrFE) nanofiber. Chromium and copper were then sputtered onto the P(VDF-TrFE) film using a magnetron sputtering machine to serve as the top electrode. A tungsten mass was affixed to the end of the beam to lower the resonant frequency. The sensor functions as a triaxial piezoelectric sensor (TPS), adept at detecting changes in acceleration, frequency, and tilting angle with remarkable precision, utilizing machine learning (ML) to achieve recognition accuracies close to 100% with resolutions of 0.01 g, 0.01 Hz, and 2° for acceleration, frequency, and tilting angle, respectively. ML-assisted TPS using three LF-PEGs enables high-precision multifunctional vibration recognition, achieving 98%–100% accuracy in detecting acceleration, frequency, and tilting angle.

The ‘Tactile Avatar’ system features an advanced tactile sensor made from piezoelectric materials designed to emulate the dynamic sensing capabilities of human skin (figure 6(c)) [38]. It utilizes a polyimide film substrate arranged in a 5×6 cell array. Photolithography was used to pattern the array on the substrate; the cell size was $1 \text{ mm} \times 1 \text{ mm}$. A 100 nm-thick Au layer and a 10 nm-thick Cr layer were deposited using an RF magnetron sputtering system. Next, a 5×6 bottom electrode array of Au was obtained through a lift-off process. P(VDF-TrFE) film was fabricated by spin coating, and the film was annealed at 130 °C for 2 h. A dome structure was created with a 3D-printed mold, and the PDMS solution was produced by mixing the base oil and hardener (10:1). Air bubbles produced by mixing were removed over 30 min in a vacuum desiccator. The solution was poured into the 3D mold and left to harden for 12 h at 60 °C. This sensor measures multiple tactile properties such as pressure, temperature, hardness, sliding velocity, and surface topography, enabling it to mimic human tactile sensations accurately. Integrated with a deep learning framework, it analyzes and categorizes materials (42 samples) by their physical characteristics, achieving high accuracy in texture classification. This sophisticated design and functionality allow the sensor to deliver nuanced tactile feedback similar to human touch, making it ideal for applications requiring detailed material discrimination.

Figure 6(d) illustrates the innovative E-skin, which employs a complex manufacturing approach, integrating a

micro-wrinkled PDMS (amplitude 15 μm , wavelength 40 μm) substrate with hybrid nanomaterials such as silver nanowires (AgNWs) and ZnO NWs [37]. The PDMS film was prepared with a PDMS prepolymer and a curing agent (weight ratio 20:1). The square PDMS substrate ($\sim 0.5 \text{ mm}$ thick) was biaxially stretched, then exposed to UVO ($28 \text{ mW}\cdot\text{cm}^{-2}$) for 60 min. The pre-strain was simultaneously released from each axial direction, inducing a randomly wrinkled PDMS substrate. A mixed solution of silver nanowires and zinc oxide nanowires was dropped on the wrinkled substrate. After the droplets evaporated, the hybrid nanomaterials were uniformly deposited on the PDMS substrate. The pre-cured PDMS (20:1) was diluted in hexane with a ratio of 3:1. The solution was spray-coated on the layer of nanomaterials, followed by the PDMS curing process. When the coated substrate was placed in an upside-down position during the curing process, the PDMS dielectric layer covered the surface of the nanomaterials layer. The piezoelectric constant is enhanced by incorporating ZnO NWs, known for their piezoelectric properties, and conductive AgNWs within the uniquely structured PDMS, which boosts surface interaction and mechanical responsiveness. When the surface energy and roughness increase while the modulus decreases, the piezoelectric voltage and the amplitude sum for frequency both rise due to the stronger adhesion force between the sensor and the contacted object. Electrical signals were collected by dragging the samples with the sensor and then performing an FFT analysis. This approach was used to compare FFT signals from PDMS samples with different textures. The sensor was able to classify the various PDMS samples with an accuracy of $(84.4 \pm 0.4)\%$ based solely on the texture information obtained. In contrast, human skin achieved a classification accuracy of $(62.2 \pm 0.5)\%$. The dielectric layers’ fingerprint-like roughness greatly enhances the sensor’s texture-sensing proficiency, increasing surface friction and adhesion, and amplifying tactile feedback. This advanced functionality makes the E-skin ideal for applications in robotics and prosthetics, where an accurate replication of human skin’s sensory capabilities is essential.

4. Manufacturing strategies for triboelectric-based intelligent sensor applications

Contact electrification occurs between any two materials, and the intensity of this contact influences the magnitude of charge transfer. Leveraging this principle, TENGs have been developed as self-powered sensors for pressure and touch applications. Traditionally, TENGs have been primarily utilized for energy harvesting rather than as standalone sensors due to their instantaneous and dynamic sensing mechanisms, which differ from conventional sensors such as capacitive or piezoresistive types. However, recent advancements have tailored TENGs to function as agile sensors, thanks to their unique properties of multi-sensing and self-powering. This section discusses TENG-based tactile and pressure sensors, emphasizing the manufacturing strategies to enhance their sensing performance.

4.1. Triboelectric-based pressure and touch sensors

One of the most demanding fields in sensing technology is robotic sensing and perception, driven by the goal of developing robust and precise methods that mimic and surpass human sensory capabilities. Figure 7(a) illustrates a smart soft robotic arm that captures continuous motion and tactile information via a gripper device [4]. The soft gripper was designed using SolidWorks and fabricated through 3D printing. The primary detection mechanism relied on contact separation for tactile and pressure sensing, with additional capabilities to detect sliding and contact. This system incorporated two TENG sensors operating in single-electrode mode to gather gripping data simultaneously. The TENG-based sensors were fabricated by arranging nickel-fabric electrodes on a PET film substrate, securing them in a mold, coating them with EcoFlex 00-30, and curing at 50 °C. The second sensor was fabricated using 3D printing and nickel-fabric coating on a gear. The soft gripper was manufactured from TPU filament, extruded at 210 °C, with precise adjustments to flow diameter and layer thickness to ensure accuracy and flexibility. Moreover, using peak counting and voltage ratio analysis from multiple electrodes, the system minimized noise and inaccuracies potentially caused by humidity and temperature fluctuations. To produce TENGs with a more precise and wide sensing range, Rasel *et al* fabricated a TENG pressure sensor with a range of 5 kPa–450 kPa and a sensitivity of 0.5 V·kPa⁻¹ by tuning the device's internal resistivity to 2.5 mΩ (figure 7(b) [136]). CNT was used in a PDMS matrix along with a sandpaper template to create microstructures on the surface. By selecting and modifying the material through surface micro-patterning, functionalization methods, and device structure optimization, an energy conversion efficiency of 48.17% was achieved. The device was then assembled inside a shoe (insole) application to detect human motion and weight. Utilizing nanopatterning as a fundamental method to enhance triboelectric perception is crucial for improving the performance of triboelectric-based sensors. In figure 7(c), the schematic of fabricating a TENG sensor based on PDMS material is depicted, where a grated compact disk mold and a hot plate, along with UV/O₃ treatment, were employed to create the nanostructured device [137]. This nanostructured device could generate double the open-circuit voltage of a planar PDMS TENG while maintaining transparency, flexibility, and stretchability. With an increased effective contact area, leading to a power density of 266 μW·cm⁻² upon touch, the TENG demonstrated its potential as a sensory platform for constructing tactile keypads.

Liu *et al* developed a ferrofluid-based triboelectric tactile sensor, which could be used as a personalized password lock with variable force requirements for security applications (figure 7(d)) [138]. An organic-ferrofluid (Neodymium (NdFeB) magnet ($D = 10$ mm)) was purchased and deposited on an aluminum foil, offering a simple, low-cost method for fabricating this TENG, which has the unique characteristic of dynamic control of the morphology of the TENG surface. A sensitivity of 21.48 kPa⁻¹ was attained with a fast response time (~90 ms) accompanied by negligible wear and tear of the TENG. The ferrofluid is positioned on an

Al film, acting as the liquid triboelectrification layer, while PTFE serves as the opposing layer, with a magnet situated beneath the device. Upon introducing a magnet, the ferrofluid undergoes deformation in response to the externally applied magnetic field. The high microstructure and low Young's modulus of the ferrofluid as the triboelectric layer enhanced sensing properties by forming a spiked structure under the influence of an external magnetic field. As the distance or angle changes, the morphology and the sensitivity of the sensor can also be changed. This demonstrates innovative material strides that can only be realized in TENG-based sensors.

Texture sensing is crucial for advanced sensing and detection in intelligent systems built on TENGs. Figure 7(e) illustrates a triboelectric tactile sensor with flower-shaped holes for texture detection [139]. Unlike previous studies that employed multiple channels for texture detection, this study utilized a single channel and a dual shielding layer, effectively recognizing multiple textures with high accuracy. The sensor comprised conventional triboelectric materials, including silicon rubber, copper, and kapton, which underwent molding and coating for device fabrication. As an object slides across the surface, voltage peaks with a low signal-to-noise ratio are generated due to the shielding layers. Subsequently, a convolutional neural network (CNN) model was developed for efficient texture recognition, achieving a recognition accuracy of 92.58% for five fruits and five vegetables in practical recognition tests. Combining triboelectric-based sensors with other devices has further extended their possibilities and sensing capabilities. For superior sensing performance, TENG-based sensors can be combined with PENG, electromagnetics, and photovoltaics. In a recent study by Yang *et al*, a novel triboelectric-optical hybrid tactile sensor (TOHTS) for human-machine tactile interaction was fabricated (figure 7(f)) [140]. The primary function of the TENG part is to receive external stimuli, while the photoelectric part converts the tactile stimuli into photoelectric signals. The device was fabricated using a simple structure involving micro-structured layers to improve sensitivity through a drop coating method in a designed mold. The TOHTS device utilizes contact electrification, electrostatic induction, and the photoelectric effect. When an external object approaches the touch layer, it disrupts electrostatic equilibrium, causing a flow of free electrons and generating a voltage in the external circuit. The device detects touch by measuring changes in voltage and adjusting light intensity accordingly for sensing. The sensor exhibited a fast response time of 9 ms and low power consumption owing to the characteristics of the unique sensing mechanism while achieving strong linearity ($R^2 \approx 0.9952$) in sensing contact force. This enables application in human-machine tactile interaction tasks such as text input and object motion control. To enhance the use of TENGs in tactile sensing, their output signals must be modulated from instantaneous and alternating to active tactile sensing devices. One way to achieve this is to integrate TENGs with transistors and use the output from the TENG to tune/control the carrier transport characteristics of the source-drain current (I_{ds}) as if a gate voltage had been applied.

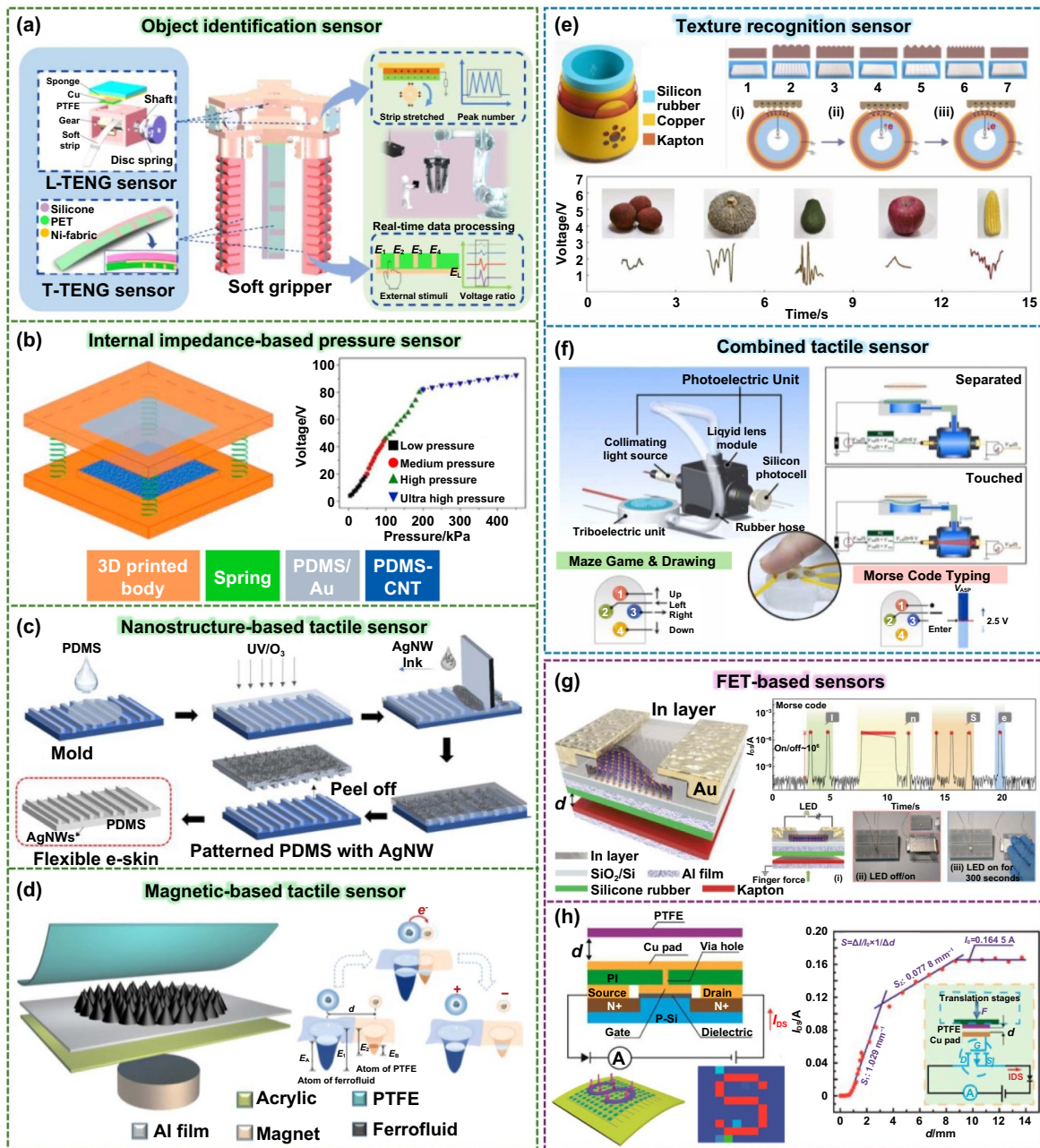


Figure 7. Manufacturing strategies of triboelectric-based pressure and touch sensors. (a) Designed and printed soft-robotic gripper system with Ni-fabric and silicone for tactile sensing. Reproduced from [4]. CC BY 4.0. (b) Fabrication of surface micro-patterned PDMS-CNT for TENG-based pressure sensor [136]. Reprinted from [136], © 2018 Elsevier Ltd. All rights reserved. (c) The manufacturing process of a nanotextured PDMS film for combined energy harvesting and tactile sensing. Reprinted with permission from [137]. Copyright (2022) American Chemical Society. (d) Development of ferrofluid-based triboelectric tactile sensor for high-sensitivity towards security applications. Reproduced from [138]. CC BY 4.0. (e) Fabrication of wearable TENG tactile sensor with patterned flower-shaped holes for texture identification [139]. Reprinted from [139], © 2023 Elsevier Ltd. All rights reserved. (f) Constructing a triboelectric-optical hybrid tactile sensor (TOHTS) with a separable modular structure for human-machine interaction [140]. Reprinted from [140], © 2024 Elsevier Ltd. All rights reserved. (g) Manufacturing a low-power consuming tactile sensor by combining an In-doped InSe transistor and triboelectric nanogenerator. [141] John Wiley & Sons. © 2019 WILEY-VCH Verlag GmbH & Co. KGaA, Weinheim. (h) Assembly of field-effect transistor units and TENGs into a 10×10 array on a polyimide substrate for active tactile sensing. Reprinted with permission from [142]. Copyright (2016) American Chemical Society.

Figure 7(g) shows an indium selenide (InSe) tribotronic transistor obtained by the direct combination of a transistor device and a TENG [141]. The device is fabricated by depositing few-layer InSe flakes on a Si substrate with a SiO₂ layer,

followed by the deposition of a 32 nm thick In layer and the patterning of source-drain contacts. An Al layer is added on the bottom of the Si substrate for ohmic contact and TENG coupling, facilitating the generation of triboelectric potential

for bias input to the FET. Significant current modulation ranging from 10^{-11} to 10^{-5} A was achieved under a low V_{ds} of 0.1 V, demonstrating a high on/off current ratio of 10^6 and low operating voltage. This meets high signal resolution and low power consumption requirements. The device demonstrated outstanding performance by transcribing Morse code and enabling convenient on/off state transformations controlled by finger touch. Additionally, it was integrated with LEDs to create tactile sensors that respond to human signals, showcasing practical features for integration into modern intelligent systems requiring tactile sensors and human-machine interfaces.

A large-scale and active tactile system was also developed by integrating multiple field-effect transistor units and TENGs into a polyimide substrate, as shown in figure 7(h) [142]. The fabrication process of the flexible tribotronic transistor array (TTA) involved cleaning and treating a PI substrate, drilling holes, depositing Cu electrodes on both sides, electroplating Ni pads, integrating microfabricated transistors and diodes, and sealing the device with PTFE film and adhesive tape. This resulted in a designed TTA with independent pixels, enabling individual modulation and control. The pixel size was scaled down from $5 \text{ mm} \times 5 \text{ mm}$ to $0.5 \text{ mm} \times 0.5 \text{ mm}$ to increase the resolution, maintaining a sensitivity of 1.029 mm^{-1} . The active tactile sensing system evaluated its capability by placing letter-shaped slabs on the sensing pixels of a flexible 10×10 TTA. Background mapping provided a reference, revealing current variations among pixels due to induced charges on the Cu pad upon contact with the PTFE film. Intensity image reconstructions showed significant current changes in pixels touching the slabs, promising real-time tactile sensing and image reconstruction.

4.2. Triboelectric-based distance and material sensors

In tactile sensors, TENGs have marked a significant advancement, offering exceptional capabilities in detecting objects remotely and distinguishing between various materials. Unlike conventional tactile sensors, TENG-based systems harness the unique principles of triboelectricity, enabling precise and sensitive measurements without requiring direct physical contact. The unique perceived output when a TENG is paired with a particular material forms the basis for materials detection sensors. In contrast, distance sensors operate based on the electric field perception of high-charge TENG surfaces. This section delves into the superior functionalities of TENGs, exploring their potential in tactile sensing applications and highlighting their crucial role in driving innovations in tactile sensing technology.

Toward the goal of an intelligent human-machine interface, Tang *et al* fabricated a triboelectric touch-free screen sensor (TSS) for non-contact gesture recognition, as shown in figure 8(a) [48]. The outlined method involves fabricating ten sensor units, each measuring $2 \text{ cm} \times 2 \text{ cm}$. These units comprise graphene, an indium tin oxide (ITO) frame, and a PET substrate. It was found that increased spacing between ITO line electrodes reduces crosstalk, maintaining high transparency (85% transmittance in visible light) and flexibility.

Monolayer graphene was grown on a copper foil via CVD, then coated with PMMA and transferred onto an ITO-coated PET substrate. Laser etching formed the ITO frame, producing a sensor unit with high-quality monolayer graphene. The lightweight, flexibility, and transparency of the graphene/ITO/PET trilayer structure allowed easy integration into the device to facilitate gesture detection. The TSS was demonstrated to detect non-contact gestures made by human fingers, directly enhancing the user experience on electronic screens.

To enhance the capabilities of contactless sensing, the surface charge density of TENG material must be improved. Zhang *et al* adopted the strategy of doping and microstructure tuning to fabricate a contactless sensor with a speed sensitivity of up to $1.175 \text{ Vs}\cdot\text{m}^{-1}$ (figure 8(b)) [46]. The fabrication involved preparing PVDF and PVDF@ $\text{Ti}_3\text{C}_2\text{T}_x$ films by dissolving PVDF particles in DMF and electrospinning the solution onto substrates under controlled humidity and voltage conditions. $\text{Ti}_3\text{C}_2\text{T}_x$ solution was incorporated into the PVDF solution for PVDF@ $\text{Ti}_3\text{C}_2\text{T}_x$ film fabrication using electrostatic spinning equipment. The assembly of PVDF@ $\text{Ti}_3\text{C}_2\text{T}_x$ -based TENG entailed using nylon and PVDF@ $\text{Ti}_3\text{C}_2\text{T}_x$ films as triboelectric materials, affixing them onto acrylic sheet substrates. Copper foil and sponge layers were added, and electrodes were connected for device operation. Incorporating electrospinning technology into the fabrication process offers advantages over traditional methods, such as simplicity, versatility, and the ability to produce nanofibers with controllable morphology. The sensor demonstrated advanced capability to detect human motion states such as running and jumping, even within a range of 70 cm.

Zheng *et al* demonstrated a strategy to fabricate non-contact triboelectric sensors for self-powered sensing and vibrational signal acquisition with high signal and bandwidth, as shown in figure 8(c) [44]. This study is based on a material improvement strategy incorporating carbon nanotubes into nitrocellulose (CNTs/NC), endowing the triboelectric layer with charge-storing capacity. This enhancement significantly boosts the triboelectric output, increasing the distance sensing capability. The fabrication of CNTs/NC involves dissolving pure NC membrane in solvents, dispersing CNTs, and evaporating the solvent to form a stratified structure. CNT dispersion liquid and CNT pastes are prepared separately, added to the NC solution, and then coated to finalize the CNTs/NC film. With this simple fabrication technique, the device achieved an optimal distance response sensitivity of $57.10 \text{ V}\cdot\text{mm}^{-1}$, a wide-bandwidth response from 0.1 to 4 000 Hz, and relative humidity stability due to the enhanced moisture resistance from the films' hydrophobic nature.

Wang *et al* employed an electrode and triboelectric material interface structure management strategy to improve the material identification accuracy of the TENG-based sensor, as represented in figure 8(d) [54]. This TENG device has an etched copper sheet and a triboelectric layer (PDMS) embedded in the etched holes. The copper sheet was etched by immersing it in ammonium hydroxide and then drying it to create a micro-surface structure. The device was fabricated by mixing PDMS prepolymer and a curing agent, pouring it onto the copper

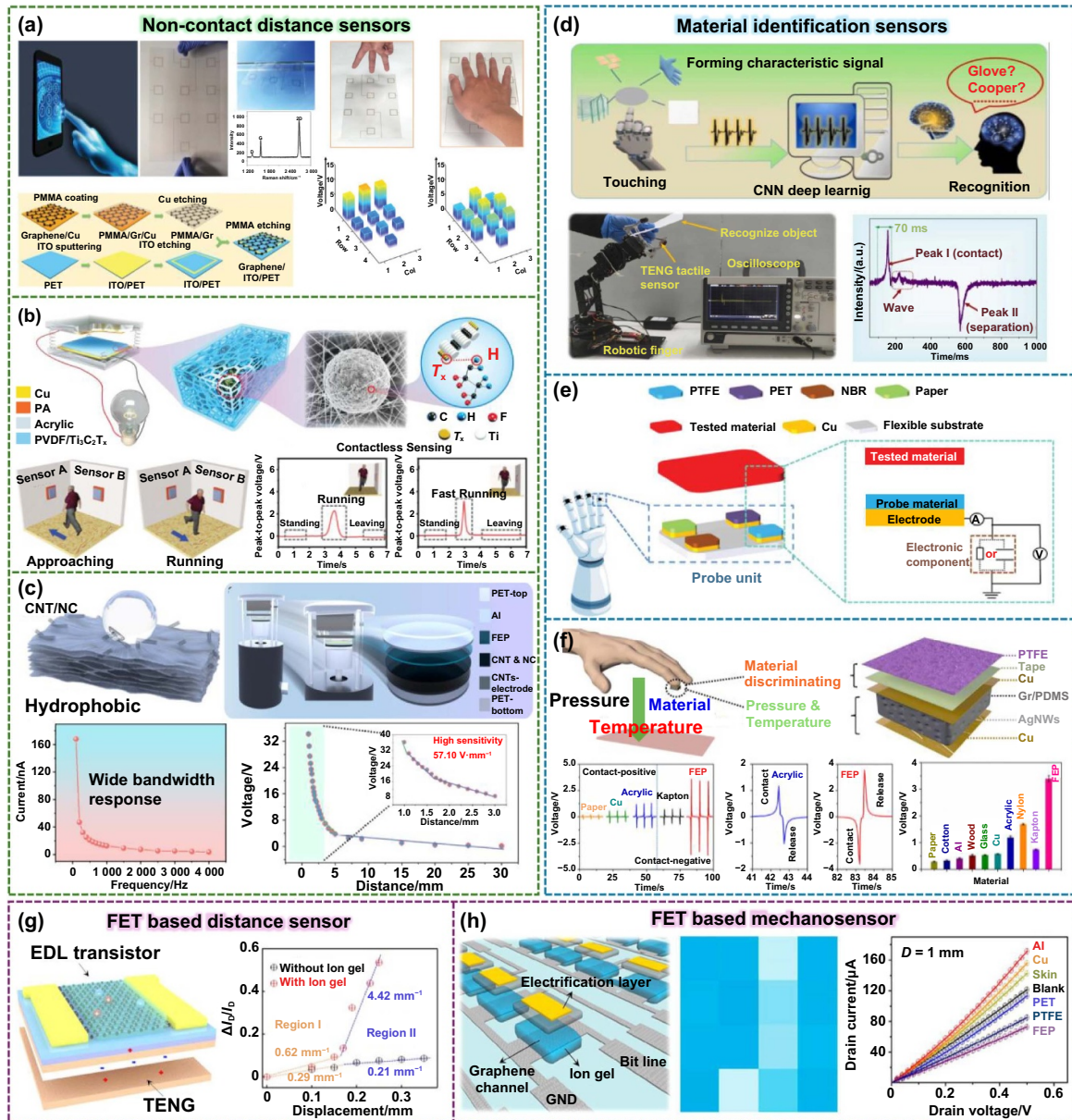


Figure 8. Manufacturing strategies of triboelectric-based distance and material sensors. (a) Fabrication of a triboelectric touch-free screen sensor with a multilayered structure using CVD and spin coating methods for noncontact gesture recognition. [48] John Wiley & Sons. © 2019 WILEY-VCH Verlag GmbH & Co. KGaA, Weinheim. (b) Controlled electrostatic spinning method utilizing a PVDF@MXene composite film for self-powered distance motion sensor. [46] John Wiley & Sons. © 2022 Wiley-VCH GmbH. (c) Composite prepared from CNT and NC for a hydrophobic surface-enhanced noncontact triboelectric sensor for vibration signal acquisition. Reprinted with permission from [44]. Copyright (2024) American Chemical Society. (d) Electrode and material tuning strategy on Cu electrode and PDMS for improved materials identification sensor [54]. Reprinted from [54], © 2024 Elsevier Ltd. All rights reserved. (e) Fabrication of an innovative flexible sensor array using four different materials for more accurate material recognition. [56] John Wiley & Sons. © 2020 Wiley-VCH GmbH. (f) Engineering and optimizing hierarchical sponge-based TENG for multifunctional tactile sensing. Reproduced from [25]. CC BY 4.0. (g) Preparation of an ion gel layer on top of a tribotronic graphene transistor for utilization as a multiparameter distance sensor. Reprinted with permission from [143]. Copyright (2020) American Chemical Society. (h) Fabrication of a mechanosensation-active matrix based on ion gel tribotronic planar graphene transistor array on a flexible PET substrate. Reprinted with permission from [144]. Copyright (2018) American Chemical Society.

sheet fixed on a glass substrate, and heating it. This produced a TENG tactile sensor with a material recognition accuracy of 99.6%. Affixed to a robotic fingertip, the TENG device collected signals via an oscilloscope for material recognition, which was then processed using CNN for precise material identification. The ML and recognition processes were conducted using

Python, with real-time analysis and display systems facilitating the sensor’s practical application for optimizing parameters and evaluating construction precautions for an artificial tactile perception smart finger.

Figure 8(e) shows a sensor array based on TENG for material recognition [56]. An innovative strategy is employed

by using different triboelectric materials on the same array. Different materials produce different charge transfers, so this method was adopted to analyze and classify materials such as plastic, glass, and metal more effectively. The probe quickly responded within 70 ms with a simple structure and conventional triboelectric materials. The single-electrode-based tactile sensor array could recognize different materials accurately using this strategy of simultaneous multimaterial sensing.

Multifunctional sensing can be achieved with TENGs for intelligent systems. Wang *et al* reported a sponge-structured film for pressure, temperature, and material identification (figure 8(f)) [25]. The device, made from hydrophobic films and a graphene/PDMS sponge, was fabricated using graphene powder, PTFE, silver nitrate, and PDMS. Hydrophobic films were produced by mixing zinc acetate, NaCl, and PTFE emulsion, then drying and curing. Graphene/PDMS composites were created by mixing PDMS with graphene powder, followed by compaction, curing, and NaCl particle removal. AgNWs were synthesized by mixing PVP, glycol, silver nitrate, and NaCl, followed by stirring and rinsing. The sensor was assembled by depositing AgNWs on Cu sheets, sandwiching graphene/PDMS composites between Cu sheets, and attaching hydrophobic PTFE films. This low-cost fabrication method resulted in a multifunctional sensor with a pressure sensing accuracy of 15.22 kPa^{-1} , temperature sensing accuracy of 1 K, and material identification capability. Such multifunctional sensors can enhance TENG-based systems by accounting for various parameters affecting output.

In figure 8(g), Zhang *et al* combined an EDL transistor and a TENG for multiparameter distance sensing [143]. This work proposes a method to enhance tribotronic gating by ion gel capacitive coupling, facilitating the development of an advanced sensing device. Fabricating a dual-mode field effect transistor improves tribotronic gating and multiparameter distance sensing capability. The device was fabricated by depositing Cr/Au on p-type Si with SiO_2 , forming electrodes via photolithography and etching, growing and transferring monolayer graphene, patterning it, photopatterning a UV-curable ionic gel, and integrating a Cu/PTFE/Cu TENG in contact-separation mode to the graphene FET's bottom Si gate. In this device, ion gel coupling enhances device performance, doubling the on-state current, quadrupling the on/off ratio, and increasing field effect mobility tenfold. This methodology offers a universal approach to enhance tribotronic potential gating, enabling the design of sophisticated sensing devices with superior performance and multifunctional sensations.

In figure 8(h), Meng *et al* introduced a mechanosensation-active matrix utilizing a direct-contact tribotronic planar graphene transistor array for sensing external stimuli and providing feedback instructions [144]. The sensor achieves highly efficient gating and sensation properties by utilizing ion gel as the dielectric in the graphene transistor and the friction layer for triboelectric potential coupling. The device fabrication process involves preparing high-quality monolayer graphene films via CVD on a Cu foil and transferring them onto a PET substrate. Standard photolithography and oxygen plasma etching techniques are used for patterning graphene. At the same time, ion gel ink is cast onto the patterned graphene to

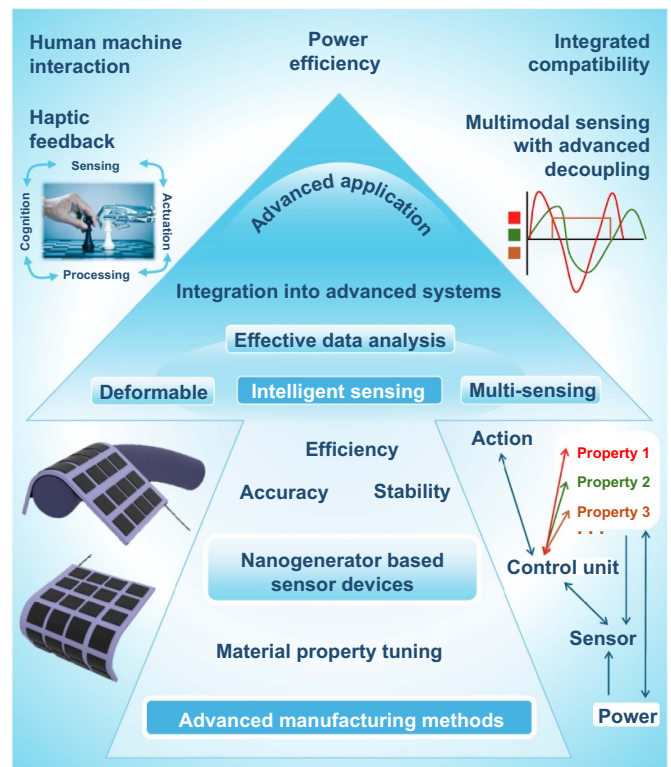


Figure 9. Advancements and challenges in the design of multifunctional tactile sensors for wearable and robotic applications.

form the active channel and source/drain electrodes. The tribotronic sensing mechanism relies on the contact-separation mode between a PTFE film and a Cu film in a TENG setup. It enables the sensor to sense approaching distances, recognize different material categories, and even distinguish voices with high sensitivity (0.16 mm^{-1}), fast response time ($\sim 15 \text{ ms}$), and excellent durability (over 1000 cycles). Additionally, the fabricated active matrix can visualize a 2D color mapping of the target object, offering a route for efficient and low-power-consuming mechanosensation in various applications, including wearable human-machine interfaces, artificial electronic skin, and telemedicine for patient surveillance.

5. Summary and perspective

This paper has reviewed and highlighted recent advances in highly sensitive tactile sensors using piezoelectric and triboelectric effects. It explains the materials and device fabrication strategies for tactile sensors using piezoelectric and triboelectric effects, as well as the types of sensory recognition. As the various application fields for tactile sensors are presented, the necessary technical challenges are becoming more apparent (figure 9).

First, future tactile sensors need to operate in irregular shapes rather than flat shapes to adapt to wearable devices, medical applications, and robotics applications, thus requiring a high degree of freedom in sensor shape. For this purpose, the components of the sensor, including the substrate, electrodes, sensor materials, and interconnectors, all need to

exhibit flexibility or stretchability. However, maintaining high performance and multifunctionalities while retaining flexibility or stretchability still shows limitations.

Additionally, to apply tactile sensors in future robots, prosthetics, and human–machine interfaces, the sensors need to simultaneously recognize various senses from a single material. Many research groups aim to mimic the human sensory nervous system, but due to the limitations of materials and decoupling technologies, there are difficulties in recognizing dynamic and static sensing in a single sensor. Consequently, it fails to meet the requirements of major senses and performances needed in various industries. As a result, integrated sensors combining multiple sensors are being implemented, but due to spatial constraints and the complexity of design, actual industrial applications are challenging. Although research on sensors that can recognize multiple senses from a single device and decoupling technology for recognizing two senses simultaneously has been reported, it is technically challenging to simultaneously recognize and decouple more than three senses. Therefore, it is necessary to develop materials and device technologies that can decouple and recognize more than three senses from a single material.

Finally, to effectively implement various operations from the diverse data collected by numerous sensors, the process can be more stable and effective if the multidimensional sensor data are learned during the operation. Previously, analyzing each sensor data to generate actions did not leverage the advantages of a large amount of sensor data, but now, through AI-based learning of multidimensional sensor data, we expect robots capable of precise operations, similar to how humans can perform delicate tasks by touch alone. It is anticipated that AI-based multi-sensory sensors will make innovative contributions to such advancements in various fields.

Acknowledgments

This work was supported by National Research Foundation of Korea (2022M3D1A2054488), and Technology Innovation Program (20025736, Development of MICS SoC and platform for *in-vivo* implantable electroceutical device) funded by the Ministry of Trade, Industry & Energy (MOTIE, Korea).

CRedit author statement

Hyosik Park and Gbadam Gerald Selasie contributed equally to this work. Hyosik Park: Conceptualization, Methodology, Writing—original draft. Gbadam Gerald Selasie: Formal analysis, Investigation, Writing—original draft. Simiao Niu: Investigation, Validation. Hanjun Ryu: Conceptualization, Supervision, Writing—review & editing. Ju-Hyuck Lee: Conceptualization, Supervision, Writing—review & editing.

ORCID iDs

Hyosik Park  <https://orcid.org/0000-0002-5656-7714>

Ju-Hyuck Lee  <https://orcid.org/0000-0001-5383-5894>

References

- [1] Pang Y K, Xu X C, Chen S E, Fang Y H, Shi X D, Deng Y M, Wang Z L and Cao C Y 2022 Skin-inspired textile-based tactile sensors enable multifunctional sensing of wearables and soft robots *Nano Energy* **96** 107137
- [2] Cheng S B, Narang Y S, Yang C H, Suo Z G and Howe R D 2019 Stick-on large-strain sensors for soft robots *Adv. Mater. Interfaces* **6** 1900985
- [3] Chin K, Hellebrekers T and Majidi C 2020 Machine learning for soft robotic sensing and control *Adv. Intell. Syst.* **2** 1900171
- [4] Jin T *et al* 2020 Triboelectric nanogenerator sensors for soft robotics aiming at digital twin applications *Nat. Commun.* **11** 5381
- [5] Won P *et al* 2021 Transparent soft actuators/sensors and camouflage skins for imperceptible soft robotics *Adv. Mater.* **33** 2002397
- [6] Pal A, Restrepo V, Goswami D and Martinez R V 2021 Exploiting mechanical instabilities in soft robotics: control, sensing, and actuation *Adv. Mater.* **33** 2006939
- [7] Luo H X *et al* 2024 Bioinspired suspended sensing membrane array with modulable wedged-conductive channels for crosstalk-free and high-resolution detection *Adv. Sci.* **11** 2403645
- [8] Li S, Chen X L, Li X M, Tian H M, Wang C H, Nie B B, He J and Shao J Y 2022 Bioinspired robot skin with mechanically gated electron channels for sliding tactile perception *Sci. Adv.* **8** eade0720
- [9] Zhong J W, Ma Y, Song Y, Zhong Q Z, Chu Y, Karakurt I, Bogy D B and Lin L W 2019 A flexible piezoelectret actuator/sensor patch for mechanical human–machine interfaces *ACS Nano* **13** 7107–16
- [10] Xu C S, Chen J, Zhu Z F, Liu M R, Lan R H, Chen X H, Tang W, Zhang Y and Li H 2024 Flexible pressure sensors in human–machine interface applications *Small* **20** 2306655
- [11] Yu S, Park T H, Jiang W, Lee S W, Kim E H, Lee S, Park J E and Park C 2023 Soft human–machine interface sensing displays: materials and devices *Adv. Mater.* **35** 2204964
- [12] Yin R Y, Wang D P, Zhao S F, Lou Z and Shen G Z 2021 Wearable sensors-enabled human–machine interaction systems: from design to application *Adv. Funct. Mater.* **31** 2008936
- [13] Wang M, Wang T, Luo Y F, He K, Pan L, Li Z, Cui Z Q, Liu Z H, Tu J Q and Chen X D 2021 Fusing stretchable sensing technology with machine learning for human–machine interfaces *Adv. Funct. Mater.* **31** 2008807
- [14] Lim H R, Kim H S, Qazi R, Kwon Y T, Jeong J W and Yeo W H 2020 Advanced soft materials, sensor integrations, and applications of wearable flexible hybrid electronics in healthcare, energy, and environment *Adv. Mater.* **32** 1901924
- [15] Lu Y Y, Yang G, Shen Y J, Yang H Y and Xu K C 2022 Multifunctional flexible humidity sensor systems towards noncontact wearable electronics *Nano-Micro. Lett.* **14** 150
- [16] Wang H Z, Li Z, Liu Z Y, Fu J K, Shan T Y, Yang X Y, Lei Q Y, Yang Y J and Li D H 2022 Flexible capacitive pressure sensors for wearable electronics *J. Mater. Chem. C* **10** 1594–605
- [17] Li L H *et al* 2018 Ultrastretchable fiber sensor with high sensitivity in whole workable range for wearable electronics and implantable medicine *Adv. Sci.* **5** 1800558
- [18] Xu K C, Lu Y Y and Takei K 2019 Multifunctional skin-inspired flexible sensor systems for wearable electronics *Adv. Mater. Technol.* **4** 1800628
- [19] Lee Y, Kim J, Jang B, Kim S, Sharma B K, Kim J H and Ahn J H 2019 Graphene-based stretchable/wearable self-powered touch sensor *Nano Energy* **62** 259–67

- [20] Feng T X, Ling D, Li C Y, Zheng W T, Zhang S C, Li C, Emel' Yanov A, Pozdnyakov A S, Lu L J and Mao Y C 2024 Stretchable on-skin touchless screen sensor enabled by ionic hydrogel *Nano Res.* **17** 4462–70
- [21] Tkachev S, Monteiro M, Santos J, Placidi E, Hassine M B, Marques P, Ferreira P, Alpuim P and Capasso A 2021 Environmentally friendly graphene inks for touch screen sensors *Adv. Funct. Mater.* **31** 2103287
- [22] Kim S J, Phung T H, Kim S, Rahman M K and Kwon K S 2020 Low-cost fabrication method for thin, flexible, and transparent touch screen sensors *Adv. Mater. Technol.* **5** 2000441
- [23] Wang Z H, Yuan X T, Yang J K, Huan Y, Gao X Y, Li Z M, Wang H and Dong S X 2020 3D-printed flexible, Ag-coated PNN-PZT ceramic-polymer grid-composite for electromechanical energy conversion *Nano Energy* **73** 104737
- [24] Cai Y W, Zhang X N, Wang G G, Li G Z, Zhao D Q, Sun N, Li F, Zhang H Y, Han J C and Yang Y 2021 A flexible ultra-sensitive triboelectric tactile sensor of wrinkled PDMS/MXene composite films for E-skin *Nano Energy* **81** 105663
- [25] Wang Y, Wu H T, Xu L, Zhang H N, Yang Y and Wang Z L 2020 Hierarchically patterned self-powered sensors for multifunctional tactile sensing *Sci. Adv.* **6** eabb9083
- [26] Kim N I *et al* 2020 Piezoelectric pressure sensor based on flexible gallium nitride thin film for harsh-environment and high-temperature applications *Sens. Actuators A* **305** 111940
- [27] Lin Y C, Duan S S, Zhu D, Li Y H, Wang B H and Wu J 2023 Self-powered and interface-independent tactile sensors based on bilayer single-electrode triboelectric nanogenerators for robotic electronic skin *Adv. Intell. Syst.* **5** 2100120
- [28] Liu Q, Wang X X, Song W Z, Qiu H J, Zhang J, Fan Z Y, Yu M and Long Y Z 2020 Wireless single-electrode self-powered piezoelectric sensor for monitoring *ACS Appl. Mater. Interfaces* **12** 8288–95
- [29] Chen X L, Shao J Y, Tian H M, Li X M, Wang C H, Luo Y S and Li S 2020 Scalable imprinting of flexible multiplexed sensor arrays with distributed piezoelectricity-enhanced micropillars for dynamic tactile sensing *Adv. Mater. Technol.* **5** 2000046
- [30] Liu X G, Liu J F, He L R, Shang Y H and Zhang C H 2022 3D printed piezoelectric-regulable cells with customized electromechanical response distribution for intelligent sensing *Adv. Funct. Mater.* **32** 2201274
- [31] Yu J R, Gao G Y, Huang J R, Yang X X, Han J, Zhang H, Chen Y H, Zhao C L, Sun Q J and Wang Z L 2021 Contact-electrification-activated artificial afferents at femtojoule energy *Nat. Commun.* **12** 1581
- [32] Qu X C, Xue J T, Liu Y, Rao W, Liu Z and Li Z 2022 Fingerprint-shaped triboelectric tactile sensor *Nano Energy* **98** 107324
- [33] Yeo H G, Jung J, Sim M, Jang J E and Choi H 2020 Integrated piezoelectric AlN thin film with SU-8/PDMS supporting layer for flexible sensor array *Sensors* **20** 315
- [34] Park H, Oh S J, Kim D, Kim M, Lee C, Joo H, Woo I, Bae J W and Lee J H 2022 Plasticized PVC-gel single layer-based stretchable triboelectric nanogenerator for harvesting mechanical energy and tactile sensing *Adv. Sci.* **9** 2201070
- [35] Lin W K, Wang B, Peng G X, Shan Y, Hu H and Yang Z B 2021 Skin-inspired piezoelectric tactile sensor array with crosstalk-free row+column electrodes for spatiotemporally distinguishing diverse stimuli *Adv. Sci.* **8** 2002817
- [36] Rostamian B, Koolani M, Abdollahzade P, Lankarani M, Falotico E, Amiri M and Thakor N V 2022 Texture recognition based on multi-sensory integration of proprioceptive and tactile signals *Sci. Rep.* **12** 21690
- [37] Lee G, Son J H, Lee S, Kim S W, Kim D, Nguyen N N, Lee S G and Cho K 2021 Fingerpad-inspired multimodal electronic skin for material discrimination and texture recognition *Adv. Sci.* **8** 2002606
- [38] Kim K, Sim M, Lim S H, Kim D, Lee D, Shin K, Moon C, Choi J W and Jang J E 2021 Tactile avatar: tactile sensing system mimicking human tactile cognition *Adv. Sci.* **8** 2002362
- [39] Su Y J *et al* 2021 Muscle fibers inspired high-performance piezoelectric textiles for wearable physiological monitoring *Adv. Funct. Mater.* **31** 2010962
- [40] Liu Y *et al* 2022 All-ceramic flexible piezoelectric energy harvester *Adv. Funct. Mater.* **32** 2209297
- [41] Jin C R, Hao N J, Xu Z, Trase I, Nie Y, Dong L, Closson A, Chen Z and Zhang J X J 2020 Flexible piezoelectric nanogenerators using metal-doped ZnO-PVDF films *Sens. Actuators A* **305** 111912
- [42] Du Y P, Wang R X, Zeng M X, Xu S J, Saeidi-Javash M, Wu W Z and Zhang Y L 2021 Hybrid printing of wearable piezoelectric sensors *Nano Energy* **90** 106522
- [43] Dai M J *et al* 2019 Two-dimensional van der Waals materials with aligned in-plane polarization and large piezoelectric effect for self-powered piezoelectric sensors *Nano Lett.* **19** 5410–6
- [44] Zheng T, Li G Z, Zhang L N, Lei Y, Huang W H, Wang J, Zhang B B, Xiang J W and Yang Y 2024 Dielectric-enhanced, high-sensitivity, wide-bandwidth, and moisture-resistant noncontact triboelectric sensor for vibration signal acquisition *ACS Appl. Mater. Interfaces* **16** 7904–16
- [45] Zhao C, Wang Z Y, Wang Y W, Qian Z A, Tan Z, Chen Q Y, Pan X X, Xu M Y and Lai Y C 2023 MXene-composite-enabled ultra-long-distance detection and highly sensitive self-powered noncontact triboelectric sensors and their applications in intelligent vehicle perception *Adv. Funct. Mater.* **33** 2306381
- [46] Zhang W L, Lu Y X, Liu T, Zhao J M, Liu Y H, Fu Q, Mo J L, Cai C C and Nie S X 2022 Spheres multiple physical network-based triboelectric materials for self-powered contactless sensing *Small* **18** 2200577
- [47] Tan F X, Xiong Y, Yu J R, Wang Y F, Li Y H, Wei Y C, Sun J, Xie X Y, Sun Q J and Wang Z L 2021 Triboelectric potential tuned dual-gate IGZO transistor for versatile sensory device *Nano Energy* **90** 106617
- [48] Tang Y J, Zhou H, Sun X P, Diao N H, Wang J B, Zhang B S, Qin C, Liang E J and Mao Y C 2020 Triboelectric touch-free screen sensor for noncontact gesture recognizing *Adv. Funct. Mater.* **30** 1907893
- [49] Liu Y X *et al* 2024 Multi-length engineering of (K, Na) NbO₃ films for lead-free piezoelectric acoustic sensors with high sensitivity *Adv. Funct. Mater.* **34** 2312699
- [50] Wang Q, Ruan T, Xu Q D, Yang B and Liu J Q 2021 Wearable multifunctional piezoelectric MEMS device for motion monitoring, health warning, and earphone *Nano Energy* **89** 106324
- [51] Lan B L, Xiao X, Carlo A D, Deng W L, Yang T, Jin L, Tian G, Ao Y, Yang W Q and Chen J 2022 Topological nanofibers enhanced piezoelectric membranes for soft bioelectronics *Adv. Funct. Mater.* **32** 2207393
- [52] Xu F, Yang J, Dong R Z, Jiang H X, Wang C H, Liu W L, Jiang Z X, Zhang X Q and Zhu G D 2021 Wave-shaped piezoelectric nanofiber membrane nanogenerator for acoustic detection and recognition *Adv. Fiber Mater.* **3** 368–80
- [53] Han J H *et al* 2018 Machine learning-based self-powered acoustic sensor for speaker recognition *Nano Energy* **53** 658–65

- [54] Wang S L, Wang S F, Jiang T, Zhao X K, Zhang W Q, Chen Z M, Li H L, Li P and Huang J J 2024 Enhancing the recognition accuracy of tactile sensor through electrode and triboelectric material interface structure management strategy *Nano Energy* **123** 109353
- [55] Song Z W *et al* 2022 A flexible triboelectric tactile sensor for simultaneous material and texture recognition *Nano Energy* **93** 106798
- [56] Rong X, Zhao J Q, Guo H, Zhen G W, Yu J H, Zhang C and Dong G F 2020 Material recognition sensor array by electrostatic induction and triboelectric effects *Adv. Mater. Technol.* **5** 2000641
- [57] Wei X L, Wang B C, Wu Z Y and Wang Z L 2022 An open-environment tactile sensing system: toward simple and efficient material identification *Adv. Mater.* **34** 2203073
- [58] Park H, Kim J and Lee J H 2022 Triboelectrification based multifunctional tactile sensors *J. Sens. Sci. Technol.* **31** 139–44
- [59] Yue Y *et al* 2018 3D hybrid porous mxene-sponge network and its application in piezoresistive sensor *Nano Energy* **50** 79–87
- [60] Zheng Q B, Lee J H, Shen X, Chen X D and Kim J K 2020 Graphene-based wearable piezoresistive physical sensors *Mater. Today* **36** 158–79
- [61] Yu R, Xia T C, Wu B, Yuan J, Ma L J, Cheng G J and Liu F 2020 Highly sensitive flexible piezoresistive sensor with 3D conductive network *ACS Appl. Mater. Interfaces* **12** 35291–9
- [62] Li J, Fang L C, Sun B H, Li X X and Kang S H 2020 Review—recent progress in flexible and stretchable piezoresistive sensors and their applications *J. Electrochem. Soc.* **167** 037561
- [63] Fiorillo A S, Critello C D and Pullano S A 2018 Theory, technology and applications of piezoresistive sensors: a review *Sens. Actuators A* **281** 156–75
- [64] He J, Zhang Y F, Zhou R H, Meng L R, Chen T, Mai W and Pan C F 2020 Recent advances of wearable and flexible piezoresistivity pressure sensor devices and its future prospects *J. Materiomics*. **6** 86–101
- [65] Zhang Q H *et al* 2018 An elastic autonomous self-healing capacitive sensor based on a dynamic dual crosslinked chemical system *Adv. Mater.* **30** 1801435
- [66] Qin J, Yin L J, Hao Y N, Zhong S L, Zhang D L, Bi K, Zhang Y X, Zhao Y and Dang Z M 2021 Flexible and stretchable capacitive sensors with different microstructures *Adv. Mater.* **33** 2008267
- [67] He X *et al* 2021 Microstructured capacitive sensor with broad detection range and long-term stability for human activity detection npj Flex. *Electron.* **5** 17
- [68] Ma Z Y, Zhang Y, Zhang K Y, Deng H and Fu Q 2023 Recent progress in flexible capacitive sensors: structures and properties *Nano Mater. Sci.* **5** 265–77
- [69] Cicek M O, Doganay D, Durukan M B, Gorur M C and Unalan H E 2021 Seamless monolithic design for foam based, flexible, parallel plate capacitive sensors *Adv. Mater. Technol.* **6** 2001168
- [70] Ha K H, Huh H, Li Z J and Lu N S 2022 Soft capacitive pressure sensors: trends, challenges, and perspectives *ACS Nano* **16** 3442–8
- [71] Tressler J F, Alkoy S and Newnham R E 1998 Piezoelectric sensors and sensor materials *J. Electroceram.* **2** 257–72
- [72] Lu C and Czanderna A W 2012 *Applications of Piezoelectric Quartz Crystal Microbalances* (Elsevier)
- [73] Bunde R L, Jarvi E J and Rosentreter J J 1998 Piezoelectric quartz crystal biosensors *Talanta* **46** 1223–36
- [74] Gao Z Q, Ren B, Fang Z Z, Kang H Q, Han J and Li J 2021 Accurate recognition of object contour based on flexible piezoelectric and piezoresistive dual mode strain sensors *Sens. Actuators A* **332** 113121
- [75] Jin C R *et al* 2021 Skin-like elastomer embedded zinc oxide nanoarrays for biomechanical energy harvesting *Adv. Mater. Interfaces* **8** 2100094
- [76] Zhang Y X, Ju F, Wei X Y, Wang D and Wang Y Y 2020 A piezoelectric tactile sensor for tissue stiffness detection with arbitrary contact angle *Sensors* **20** 6607
- [77] Su H X, Wang X B, Li C Y, Wang Z F, Wu Y H, Zhang J W, Zhang Y Z, Zhao C L, Wu J G and Zheng H W 2021 Enhanced energy harvesting ability of polydimethylsiloxane-BaTiO₃-based flexible piezoelectric nanogenerator for tactile imitation application *Nano Energy* **83** 105809
- [78] Zhang P, Zhang W K, Deng L and Zhang H H 2021 A triboelectric nanogenerator based on temperature-stable high dielectric BaTiO₃-based ceramic powder for energy harvesting *Nano Energy* **87** 106176
- [79] Fukada E and Yasuda I 1957 On the piezoelectric effect of bone *J. Phys. Soc. Japan* **12** 1158–62
- [80] Shamos M H, Lavine L S and Shamos M I 1963 Piezoelectric effect in bone *Nature* **197** 81
- [81] Park H, Kim Y, Kim Y, Lee C, Park H, Joo H, Lee J H and Lee J H 2023 Self-assembly of unidirectionally polarized piezoelectric peptide nanotubes using environmentally friendly solvents *Appl. Surf. Sci.* **618** 156588
- [82] Kholkin A, Amdursky N, Bdkin I, Gazit E and Rosenman G 2010 Strong piezoelectricity in bioinspired peptide nanotubes *ACS Nano* **4** 610–4
- [83] Wu T, Song Y H, Shi Z Q, Liu D N, Chen S L, Xiong C X and Yang Q L 2021 High-performance nanogenerators based on flexible cellulose nanofibril/MoS₂ nanosheet composite piezoelectric films for energy harvesting *Nano Energy* **80** 105541
- [84] Song Y H, Shi Z Q, Hu G H, Xiong C X, Isogai A and Yang Q L 2021 Recent advances in cellulose-based piezoelectric and triboelectric nanogenerators for energy harvesting: a review *J. Mater. Chem. A* **9** 1910–37
- [85] Zhang J H *et al* 2022 Finger-inspired rigid-soft hybrid tactile sensor with superior sensitivity at high frequency *Nat. Commun.* **13** 5076
- [86] Tang W, Sun Q J and Wang Z L 2023 Self-powered sensing in wearable electronics—a paradigm shift technology *Chem. Rev.* **123** 12105–34
- [87] Lin X D, Feng Z Y, Xiong Y, Sun W W, Yao W C, Wei Y C, Wang Z L and Sun Q J 2024 Piezotronic neuromorphic devices: principle, manufacture, and applications *Int. J. Extrem. Manuf.* **6** 032011
- [88] Yu J R, Yang X X and Sun Q J 2020 Piezo/tribotronics toward smart flexible sensors *Adv. Intell. Syst.* **2** 1900175
- [89] Niu S M and Wang Z L 2015 Theoretical systems of triboelectric nanogenerators *Nano Energy* **14** 161–92
- [90] Shao Z C, Chen J S, Xie Q and Mi L W 2023 Functional metal/covalent organic framework materials for triboelectric nanogenerator *Coord. Chem. Rev.* **486** 215118
- [91] Zhang R Y and Olin H 2020 Material choices for triboelectric nanogenerators: a critical review *EcoMat* **2** e12062
- [92] Zhang B B *et al* 2017 Self-powered acceleration sensor based on liquid metal triboelectric nanogenerator for vibration monitoring *ACS Nano* **11** 7440–6
- [93] Joo H, Gwak S, Park H, Yoon H J, Ryu H, Han S A and Lee J H 2024 Engineering self-healable and biodegradable ionic polyurethane with highly tribopositive behavior *Nano Energy* **126** 109706
- [94] Joo H, Gwak S, Lee M H, Park H, Lee C, Lee J H, Han S A and Lee J H 2023 Functionalized thermoplastic polyurethane with tunable tribopolarity and biodegradability for high performance and biodegradable

- triboelectric nanogenerator *Sustain. Mater. Technol.* **36** e00638
- [95] Kim J, Lee J H, Ryu H, Lee J H, Khan U, Kim H, Kwak S S and Kim S W 2017 High-performance piezoelectric, pyroelectric, and triboelectric nanogenerators based on P(VDF-TrFE) with controlled crystallinity and dipole alignment *Adv. Funct. Mater.* **27** 1700702
- [96] Chen X X, Han M D, Chen H T, Cheng X L, Song Y, Su Z M, Jiang Y G and Zhang H X 2017 A wave-shaped hybrid piezoelectric and triboelectric nanogenerator based on P(VDF-TrFE) nanofibers *Nanoscale* **9** 1263–70
- [97] Ma X, Li S Y, Dong S J, Nie J H, Iwamoto M, Lin S Q, Zheng L and Chen X Y 2019 Regulating the output performance of triboelectric nanogenerator by using P(VDF-TrFE) Langmuir monolayers *Nano Energy* **66** 104090
- [98] Guo M L, Wang C, Yang Z C, Xu Z T, Yang M S, Zhao P K, Zhou Y, Li P Y, Wang Q D and Li Y 2022 Controllable and scalable fabrication of superhydrophobic hierarchical structures for water energy harvesting *Electronics* **11** 1651
- [99] Park H, Oh S J, Kim M, Lee C, Joo H, Bae J W and Lee J H 2023 Plasticizer structural effect for sustainable and high-performance PVC gel-based triboelectric nanogenerators *Nano Energy* **114** 108615
- [100] Kim M, Park H, Lee M H, Bae J W, Lee K Y, Lee J H and Lee J H 2023 Stretching-insensitive stretchable and biocompatible triboelectric nanogenerators using plasticized PVC gel and graphene electrode for body-integrated touch sensor *Nano Energy* **107** 108159
- [101] Mao Y Y, Li Y, Xie J Y, Liu H, Guo C J and Hu W B 2021 Triboelectric nanogenerator/supercapacitor in-one self-powered textile based on PTFE yarn wrapped PDMS/MnO₂NW hybrid elastomer *Nano Energy* **84** 105918
- [102] Ouyang R, Huang Y, Ye H T, Zhang Z J and Xue H 2022 Copper particles-PTFE tube based triboelectric nanogenerator for wave energy harvesting *Nano Energy* **102** 107749
- [103] Liu H W, Dong J, Zhou H Y, Yang X D, Xu C Y, Yao Y Q, Zhou G D, Zhang S M and Song Q L 2021 Real-time acid rain sensor based on a triboelectric nanogenerator made of a PTFE-PDMS composite film *ACS Appl. Electron. Mater.* **3** 4162–71
- [104] Qiu G R, Lu L, Lu Y and Sun C W 2020 Effects of pulse charging by triboelectric nanogenerators on the performance of solid-state lithium metal batteries *ACS Appl. Mater. Interfaces* **12** 28345–50
- [105] Cheong J Y, Koay J S C, Chen R H, Aw K C, Velayutham T S, Chen B H, Li J, Foo C Y and Gan W C 2021 Maximizing the output power density enhancement of solid polymer electrolyte based-triboelectric nanogenerators via contact electrification-induced ionic polarization *Nano Energy* **90** 106616
- [106] Uzabakiriho P C *et al* 2020 High-performance, mechanically and thermally compliant silica-based solid polymer electrolyte for triboelectric nanogenerators application *Adv. Mater. Technol.* **5** 2000303
- [107] Yang W Q, Xiao P, Ni F, Zhang C, Gu J C, Kuo S W, Liu Q Q and Chen T 2022 Biomass-derived nanostructured coatings based on cellulose nanofibers-melanin hybrids toward solar-enabled multifunctional energy management *Nano Energy* **97** 107180
- [108] Contreras-Pereda N, Suárez-García S, Pfaltner R and Ruiz-Molina D 2024 Melanin-inspired conductive thin films for multimodal-sensing wearable on-skin electronics *Mater. Today Chem.* **35** 101855
- [109] Kim J, Ryu H, Lee J H, Khan U, Kwak S S, Yoon H J and Kim S W 2020 High permittivity CaCu₃Ti₄O₁₂ particle-induced internal polarization amplification for high performance triboelectric nanogenerators *Adv. Energy Mater.* **10** 1903524
- [110] Kim M P, Ahn C W, Lee Y, Kim K, Park J and Ko H 2021 Interfacial polarization-induced high-k polymer dielectric film for high-performance triboelectric devices *Nano Energy* **82** 105697
- [111] Habib M, Lantgios I and Hornbostel K 2022 A review of ceramic, polymer and composite piezoelectric materials *J. Appl. Phys.* **55** 423002
- [112] Wang R X, Sui J and Wang X D 2022 Natural piezoelectric biomaterials: a biocompatible and sustainable building block for biomedical devices *ACS Nano* **16** 17708–28
- [113] Wang X D, Song J H, Liu J and Wang Z L 2007 Direct-current nanogenerator driven by ultrasonic waves *Science* **316** 102–5
- [114] Oh H and Dayeh S A 2020 Physics-based device models and progress review for active piezoelectric semiconductor devices *Sensors* **20** 3872
- [115] Xu Q, Wen J and Qin Y 2021 Development and outlook of high output piezoelectric nanogenerators *Nano Energy* **86** 106080
- [116] Hu Y F and Wang Z L 2015 Recent progress in piezoelectric nanogenerators as a sustainable power source in self-powered systems and active sensors *Nano Energy* **14** 3–14
- [117] Chang C J, Lee Y H, Dai C A, Hsiao C C, Chen S H, Nurmalasari N P D, Chen J C, Cheng Y Y, Shih W P and Chang P Z 2011 A large area bimaterial sheet of piezoelectric nanogenerators for energy harvesting: effect of RF sputtering on ZnO nanorod *Microelectron. Eng.* **88** 2236–41
- [118] Mondal A, Singh H H and Khare N 2023 Effect of piezoelectric coefficient and dielectric constant on the performance of polymer nanocomposite piezoelectric nanogenerator *J. Mater. Sci.: Mater. Electron.* **34** 314
- [119] Hwang G T *et al* 2016 Self-powered wireless sensor node enabled by an aerosol-deposited PZT flexible energy harvester *Adv. Energy Mater.* **6** 1600237
- [120] Liu Y, Shen B Z, Bian L, Hao J G, Yang B, Zhang R and Cao W W 2023 Enhanced electromechanical performance in lead-free (Na, K) NbO₃-based piezoceramics via the synergistic design of texture engineering and sm-modification *ACS Appl. Mater. Interfaces* **15** 47221–8
- [121] Kou Q W, Yang B, Lei H B, Yang S, Zhang Z R, Liu L J, Xie H, Sun Y, Chang Y F and Li F 2023 Lead-free textured ceramics with ultrahigh piezoelectric properties by synergistic design *ACS Appl. Mater. Interfaces* **15** 37706–16
- [122] Yang L J, Chi S, Dong S P, Yuan F, Wang Z D, Lei J X, Bao L X, Xiang J and Wang J L 2020 Preparation and characterization of a novel piezoelectric nanogenerator based on soluble and meltable copolyimide for harvesting mechanical energy *Nano Energy* **67** 104220
- [123] Panda S, Hajra S, Jeong H, Panigrahi B K, Pakawanit P, Dubal D, Hong S and Kim H J 2022 Biocompatible CaTiO₃-PVDF composite-based piezoelectric nanogenerator for exercise evaluation and energy harvesting *Nano Energy* **102** 107682
- [124] Islam M N *et al* 2023 Boosting piezoelectricity by 3D printing PVDF-MoS₂ composite as a conformal and high-sensitivity piezoelectric sensor *Adv. Funct. Mater.* **33** 2302946
- [125] Sun X, Liu Y J, Luo N, Liu Y, Feng Y G, Chen S G and Wang D A 2022 Controlling the triboelectric properties and tribological behavior of polyimide materials via plasma treatment *Nano Energy* **102** 107691
- [126] Li S Y, Fan Y, Chen H Q, Nie J H, Liang Y X, Tao X L, Zhang J, Chen X Y, Fu E G and Wang Z L 2020 Manipulating the triboelectric surface charge density of

- polymers by low-energy helium ion irradiation/implantation *Energy Environ. Sci.* **13** 896–907
- [127] Ahn J *et al* 2021 Morphology-controllable wrinkled hierarchical structure and its application to superhydrophobic triboelectric nanogenerator *Nano Energy* **85** 105978
- [128] Sun J Z, Choi H, Cha S, Ahn D, Choi M, Park S, Cho Y, Lee J, Park T E and Park J J 2022 Highly enhanced triboelectric performance from increased dielectric constant induced by ionic and interfacial polarization for chitosan based multi-modal sensing system *Adv. Funct. Mater.* **32** 2109139
- [129] Tang W, Meng B and Zhang H X 2013 Investigation of power generation based on stacked triboelectric nanogenerator *Nano Energy* **2** 1164–71
- [130] Chun J, Ye B U, Lee J W, Choi D, Kang C Y, Kim S W, Wang Z L and Baik J M 2016 Boosted output performance of triboelectric nanogenerator via electric double layer effect *Nat. Commun.* **7** 12985
- [131] Cheng L, Xu Q, Zheng Y B, Jia X F and Qin Y 2018 A self-improving triboelectric nanogenerator with improved charge density and increased charge accumulation speed *Nat. Commun.* **9** 3773
- [132] Liu Q J, Jin L, Zhang P, Zhang B B, Li Y X, Xie S and Li X H 2021 Nanofibrous grids assembled orthogonally from direct-written piezoelectric fibers as self-powered tactile sensors *ACS Appl. Mater. Interfaces* **13** 10623–31
- [133] Lu J L *et al* 2022 A biodegradable and recyclable piezoelectric sensor based on a molecular ferroelectric embedded in a bacterial cellulose hydrogel *ACS Nano* **16** 3744–55
- [134] Yu D, Zheng Z P, Liu J D, Xiao H Y, Huangfu G and Guo Y P 2021 Superflexible and lead-free piezoelectric nanogenerator as a highly sensitive self-powered sensor for human motion monitoring *Nano-Micro. Lett.* **13** 117
- [135] Huang M J, Zhu M L, Feng X W, Zhang Z X, Tang T Y, Guo X G, Chen T, Liu H C, Sun L N and Lee C 2023 Intelligent cubic-designed piezoelectric node (iCUPE) with simultaneous sensing and energy harvesting ability toward self-sustained artificial intelligence of things (AIoT) *ACS Nano* **17** 6435–51
- [136] Rasel M S, Maharjan P, Salauddin M, Rahman M T, Cho H O, Kim J W and Park J Y 2018 An impedance tunable and highly efficient triboelectric nanogenerator for large-scale, ultra-sensitive pressure sensing applications *Nano Energy* **49** 603–13
- [137] Pratap A, Gogurla N and Kim S 2022 Elastic and skin-contact triboelectric nanogenerators and their applicability in energy harvesting and tactile sensing *ACS Appl. Electron. Mater.* **4** 1124–31
- [138] Liu J Y, Wen Z, Lei H, Gao Z Q and Sun X H 2022 A liquid–solid interface-based triboelectric tactile sensor with ultrahigh sensitivity of 21.48 kPa^{-1} *Nano-Micro. Lett.* **14** 88
- [139] Xing P C, An S S, Wu Y H, Li G, Liu S Z, Wang J, Cheng Y L, Zhang Y S and Pu X J 2023 A triboelectric tactile sensor with flower-shaped holes for texture recognition *Nano Energy* **116** 108758
- [140] Yang H, Bu T Z, Liu W B, Liu J Q, Ling Y Z, Wu M X, Liu W R, Wang C G, Gao X F and Wang L H 2024 A novel triboelectric-optical hybrid tactile sensor for human-machine tactile interaction *Nano Energy* **125** 109592
- [141] Li M J *et al* 2019 Low-voltage operational, low-power consuming, and high sensitive tactile switch based on 2D layered InSe tribotronics *Adv. Funct. Mater.* **29** 1809119
- [142] Yang Z W, Pang Y K, Zhang L M, Lu C X, Chen J, Zhou T, Zhang C and Wang Z L 2016 Tribotronic transistor array as an active tactile sensing system *ACS Nano* **10** 10912–20
- [143] Zhang H, Yu J R, Yang X X, Gao G Y, Qin S S, Sun J, Ding M, Jia C K, Sun Q J and Wang Z L 2020 Ion gel capacitively coupled tribotronic gating for multiparameter distance sensing *ACS Nano* **14** 3461–8
- [144] Meng Y F, Zhao J Q, Yang X X, Zhao C L, Qin S S, Cho J H, Zhang C, Sun Q J and Wang Z L 2018 Mechanosensation-active matrix based on direct-contact tribotronic planar graphene transistor array *ACS Nano* **12** 9381–9